
OptiProxy-NAS: Optimization Proxy based End-to-End Neural Architecture Search

Bo Lyu¹ Yu Cui¹ Tuo Shi¹ Ke Li²

Abstract

Neural architecture search (NAS) is a hard computationally expensive optimization problem with a discrete, vast, and spiky search space. One of the key research efforts dedicated to this space focuses on accelerating NAS via certain proxy evaluations of neural architectures. Different from the prevalent predictor-based methods using surrogate models and differentiable architecture search via supernetworks, we propose an *optimization proxy* to streamline the NAS as an end-to-end optimization framework, named OptiProxy-NAS. In particular, using a proxy representation, the NAS space is reformulated to be continuous, differentiable, and smooth. Thereby, any differentiable optimization method can be applied to the gradient-based search of the relaxed architecture parameters. Our comprehensive experiments on 12 NAS tasks of 4 search spaces across three different domains including computer vision, natural language processing, and resource-constrained NAS fully demonstrate the superior search results and efficiency. Further experiments on low-fidelity scenarios verify the flexibility.

1. Introduction

Neural architecture search (NAS) aims to automate the design of high-performing neural architectures for specific tasks. It has been successfully employed to conduct a *de-novo* design of neural network architectures that offer better accuracy versus latency trade-offs than the best human-engineered alternatives. On the other hand, NAS has an enormously large discrete architecture search space with non-convex and isolated optimum fitness landscape, making it notoriously challenging. There have been significant efforts on NAS sampling algorithm based on black-box optimization techniques, including evolutionary algorithm (EA) (Sun et al., 2020; Wei et al., 2023), Bayesian optimization (BO) (White et al., 2021a), and reinforcement learning

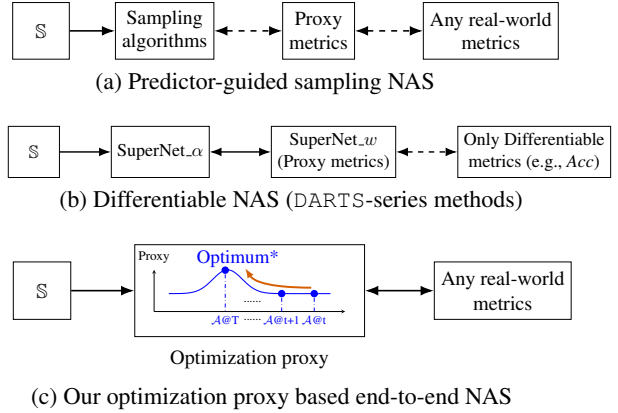


Figure 1: Schematic of the search framework comparison.

(RL) (Zoph & Le, 2017; Zoph et al., 2018). Because the performance evaluation of each candidate architecture requires a computationally demanding deep neural networks training routine, a long-standing open problem in NAS research is how to strike a balance between the trade-off of the search efficiency and the quality of the obtained architectures. We refer the interested readers to two pieces of excellent survey papers (Xie et al., 2021; White et al., 2023) for more detailed discussions.

In recent years, NAS techniques converge to two routines.

- The first one focuses on developing proxy metrics as predictors to guide the architecture sampling while maintaining a limited evaluation cost, as illustrated in Figure 1(a). Representative proxies include surrogate models (Wei et al., 2023; White et al., 2021a;c), learning curve extrapolation (Yan et al., 2021), and zero-cost metrics (Zhou et al., 2020; Abdelfattah et al., 2021). However, these proxies have been criticized for their unreliable modeling capability, evaluation biases, and inconsistent performance across tasks (White et al., 2022). The predictor-guided sampling NAS still requires a significant number of full training iterations of architectures (White et al., 2023).
- The other one mainly uses one-shot methods to reduce the overall evaluation cost. Its basic idea is to train a supernetwork (DARTS-series (Liu et al., 2019; Xie

¹Zhejiang Lab, Hangzhou, China ²Department of Computer Science, University of Exeter, Exeter, UK. Correspondence to: Bo Lyu <bo.lyu@zhejianglab.org>, Ke Li <k.li@exeter.ac.uk>.

et al., 2019; Ye et al., 2022; Cai et al., 2019)) or hypernetwork (SMASH (Brock et al., 2018b)) and then use that to provide a quick individual (subnetwork) evaluation. As illustrated in Figure 1(b), DARTS-series methods (Liu et al., 2019; Xie et al., 2019; Ye et al., 2022) construct a supernet to enable differentiable optimization over relaxed architectural variables, where the loss function serves as a proxy for *accuracy*. However, this formulation inherently makes it challenging to incorporate non-differentiable metrics, such as *latency* and *power*, along with high memory consumption in practical search (Xie et al., 2021; White et al., 2023).

Given these limitations, we contend to reach the trade-off between full-pipeline resource cost and resulting practically deployable architectures, not only optimized for *accuracy* but also account for customizable objectives such as resource constraints, runtime latency, and other deployment-specific metrics. Unlike previous efforts primarily centered on constructing proxies for costly real-world evaluation metrics, such as the *architecture-accuracy* mapping, we come up with a different hypothesis as follows.

💡 *If the NAS space is represented by a proxy space that is continuous, differentiable, and smooth—particularly one that provides a well-structured representation of high-performance regions—the search process can become more targeted and directly guided by real-world metrics, even enabling gradient-based optimization.*

Building upon this hypothesis, this paper proposes a Optimization-Proxy based end-to-end NAS framework, dubbed as OptiProxy-NAS.

- The basic idea of OptiProxy-NAS is to synthesize the prediction and search into an *optimization proxy*, which formulates NAS as an end-to-end optimization problem in a differentiable way.
- OptiProxy-NAS does not require a proxy representation of the entire space. Instead, it progressively models the NAS landscape by starting from a coarse estimation and refining it towards the precise promising regions with the search progression.
- OptiProxy-NAS is flexible as it enables a direct incorporation of any real-world NAS metrics, e.g., latency constraint and low-fidelity evaluation metrics.

Generally speaking, OptiProxy-NAS is featured in the following three advantages.

- As illustrated in Figure 1(c), our end-to-end differentiable optimization enables the gradient information flow among the discrete search space, the *optimization proxy* and any real-world metrics. Comparatively, as predictor-guided sampling NAS shown in Figure 1(a), the samplers (RL, EA, or BO) operate in discrete space and are isolated with proxy metrics, preventing direct

gradient flow. Thus, we ensure superior sampling efficiency compared to them.

- Unlike DARTS-series methods, our *optimization proxy* reduces the disparity between the discrete architecture space and real-world metrics. It avoids costly supernet networks, and expands the search beyond merely differentiable objectives, such as *accuracy*. This makes it more suitable for not only the deployment platform-aware NAS scenarios (typically involving both differentiable and non-differentiable search objectives) but also the resource-sensitive scenarios in the search process itself.
- Our *optimization proxy* relies merely on the labeled DAG representation of architecture, a standard encodings scheme in NAS. This ensures a wide applicability of OptiProxy-NAS across various search spaces.

The performance of OptiProxy-NAS is validated in a comprehensive experiment covering diverse scenarios, including 6 single-objective spaces and 6 multi-objective cases, a large space with up to 10^{53} architectures and 12 NAS tasks ranging from CV, NLP, resource-constrained (under hardware-aware metrics of deployment devices), to multi-fidelity. The results fully demonstrate the effectiveness and superiority of OptiProxy-NAS against 15 state-of-the-art (SOTA) peer algorithms. Specifically, ► on NAS-Bench-201 (Dong & Yang, 2020), we consistently achieve the optimum with nearly 100% less query cost across all tasks; ► on NAS-Bench-301 (Siems et al., 2020) and NAS-Bench-NLP (Klyuchnikov et al., 2022), we achieve significantly superior results and 400% efficiency improvement; ► on HW-NAS-Bench (Li et al., 2021), under 12 latency-constrained settings, across 6 hardware devices, our results are consistently the best comparing to the published best results with the same queries, and outperforms SOTA methods in all 12 device settings even with 50% fewer queries; ► we also experimentally show the compatibility and flexibility of OptiProxy-NAS under low-fidelity evaluation settings, and with 4 types of proxy models. In particular, OptiProxy-NAS adds merely 20 seconds and 10MB of additional memory, costing only 0.037% runtime and 0.25% memory of the total NAS pipeline. Our code will be released at <https://github.com/blyucs/OptiProxy-NAS>.

2. Proposed Method

2.1. Problem Formulation

Conventionally, NAS is formulated as a bi-level optimization problem within the discrete space:

$$\begin{aligned} \max_{\mathcal{A} \in \mathbb{S}} \quad & \text{Eval}(\langle \mathcal{A}, w^*(\mathcal{A}) \rangle; \mathbb{D}_{\text{val}}) \\ \text{s.t.} \quad & w^*(\mathcal{A}) = \arg \min_w \mathcal{L}(w(\mathcal{A}); \mathbb{D}_{\text{train}}), \end{aligned} \tag{1}$$

where \mathcal{A} stands for the architecture and \mathbb{S} represents the architecture space, the lower-level optimization focuses on the training of the candidate architectures on $\mathbb{D}_{\text{train}}$ and \mathcal{L} is a loss function, while the upper-level optimization aims to search for a neural architecture that maximizes the evaluation accuracy on \mathbb{D}_{val} , denoted as f . Following predictor-based NAS works (Wen et al., 2020; Wei et al., 2023; Dudziak et al., 2020; White et al., 2021a), given the model \hat{f} (with parameters θ) that provides the approximate representation of the landscape of f , the NAS problem can be approximated as:

$$\max_{\mathcal{A} \in \mathbb{S}} \hat{f}(\mathcal{A}, \theta^*), \quad (2)$$

where θ^* denotes the optimal parameters of f . Given that we focus solely on the differentiable models, which are proven to be effective as metric predictors, to reach an ideal model (θ^*) is infeasible due to the astronomical combinatorial space. Instead, we may approximately solve it by empirical risk minimization, formulated as:

$$\begin{aligned} & \max_{\mathcal{A} \in \mathbb{S}} \hat{f}(\mathcal{A}, \theta^*) \\ \text{s.t. } & \theta^* = \underset{\theta}{\operatorname{argmin}} \sum_{\mathcal{A} \in \mathcal{D}} \mathcal{L}(\hat{f}_{\theta}(\mathcal{A}), f(\mathcal{A})), \end{aligned} \quad (3)$$

where \mathcal{L} is the empirical loss function, and $\mathcal{D} = \{(\mathcal{A}_i, f(\mathcal{A}_i))\}_{i=1}^B$ is the sampled dataset on \mathbb{S} . Specifically, the upper-level optimization is the maximization of \hat{f} over \mathcal{A} , while the lower-level optimization includes fitting the model on \mathcal{D} . Back to NAS space, the network architectures can be parameterized by operations features (candidate operation choices) \mathcal{A}_o and the topological structure \mathcal{A}_t . Even \hat{f} is capable of fitting the landscape to be continuous, \mathcal{A}_o and \mathcal{A}_t are both discrete, thus the space remains discrete. Borrowed from (Xie et al., 2019; Cai et al., 2019; Liu et al., 2019), we have \mathcal{A}_o and \mathcal{A}_t follow a probability distribution α and β , respectively, allowing the architecture variable to be relaxed. We denote this continuous space spanning by α and β as \mathcal{X} , the proxy space. Thus, the optimization problem is reformulated as:

$$\begin{aligned} & \max_{(\alpha, \beta) \in \mathcal{X}} \hat{f}(s(\alpha, \beta), \theta^*), \\ \text{s.t. } & \theta^* = \underset{\theta}{\operatorname{argmin}} \sum_{\mathcal{A} \in \mathcal{D}} \mathcal{L}(\hat{f}_{\theta}(\mathcal{A}), f(\mathcal{A})) \\ & \mathcal{D} = \{(\mathcal{A}_b, f(\mathcal{A}_b))\}_{b=1}^B, \\ & \mathcal{A}_b \sim s(\alpha, \beta), \end{aligned} \quad (4)$$

where s is the architecture sampling function. The lower-level optimization targets θ (model fitting), depending on the data \mathcal{D} that collected by s following α, β . The upper-level optimization focuses on α, β . Although this formulation keeps the form of bi-level optimization, both the upper- and lower-level optimizations target parts of the $\hat{f}(\cdot)$, namely

Algorithm 1 Optimization Proxy based Architecture Search

- 1: **Input:** $(\alpha, \beta), \hat{f}_{\theta^*}$;
 - 2: **Parameters:** $oEpochs, tEpochs, searchEpochs$, Initial Gumbel Temperature τ , learning rate η_1, η_2 ;
 - 3: **Output:** The promising architecture batch $\{\mathcal{A}_b\}_{b=1}^Q$;
 - 4: Fix the proxy model weights θ^* ;
 - 5: **for** $e = 1$ to $searchEpochs$ **do**
 - 6: $\hat{s}_o, \hat{s}_t \leftarrow \hat{s}(\alpha), \hat{s}(\beta)$; ▷ Proxy sampling
 - 7: $\text{out} \leftarrow \hat{f}_{\theta^*}(\hat{s}_o, \hat{s}_t)$; ▷ Forward
 - 8: $\text{loss} \leftarrow \text{out}()$; ▷ Output maximization
 - 9: $\text{loss.backward}()$ to achieve $\nabla_{\alpha} \psi(\alpha, \beta), \nabla_{\beta} \psi(\alpha, \beta)$; ▷ Gradients calculated
 - 10: Alternatively call: ▷ Gradients applied
 - $\alpha_{t+1} = \alpha_t + \eta_1 \nabla_{\alpha} \psi(\alpha, \beta, \theta^*)$;
 - $\beta_{t+1} = \beta_t + \eta_2 \nabla_{\beta} \psi(\alpha, \beta, \theta^*)$;
 - for $oEpochs$ and $tEpochs$ intervals, respectively.
 - 11: Decay the τ ;
 - 12: **end for**
 - 13: $\{\mathcal{A}_b\}_{b=1}^Q \leftarrow s(\alpha^*, \beta^*)$ by Eq. (5),(6). ▷ Sampling
-

the input variables and weights, it can be solved end-to-end based on gradients. Borrowed from (Chen et al., 2021), we treat this search paradigm as ‘‘Optimization Proxy’’ for NAS.

2.2. Gradient-based Search in Optimization Proxy

Our design of the search commences with the sampling function $s(\alpha, \beta)$. First, we have \mathcal{A}_o follows a categorical distribution with the probability vector set $\alpha \in \mathbb{R}^{N \times M}$, N represents feature nodes number and M is the candidate operation number, for node i :

$$\mathcal{A}_o^i \sim \text{Cat}(\text{softmax}(\alpha^i)), \quad (5)$$

where $\text{softmax}(\alpha^i) = (p^0, p^1, \dots, p^{M-1})$ represents the sampling probabilities of each of the M candidate operations, $0 \leq p^j \leq 1$ and $\sum_{j=0}^{M-1} p^j = 1$.

Further, we have \mathcal{A}_t distributed according to a Bernoulli distribution with $\beta \in \mathbb{R}^{N \times N}$, for a specific connection:

$$\mathcal{A}_t^{(h,k)} \sim \text{Bernoulli}(\sigma(\beta^{(h,k)})), \quad (6)$$

where $\sigma(\beta^{(h,k)})$ denotes the occurrence probability of the connection between node h and k , within the range of $[0, 1]$. Following Eq. (4), the architecture search is to maximize the objective function $\psi = \hat{f}(s(\alpha, \beta), \theta^*)$. The gradients of the objective function w.r.t α and β are as follow:

$$\nabla_{\alpha} \psi = \frac{\partial \hat{f}}{\partial s} \cdot \frac{\partial s}{\partial \alpha}, \quad \nabla_{\beta} \psi = \frac{\partial \hat{f}}{\partial s} \cdot \frac{\partial s}{\partial \beta}, \quad (7)$$

where $\partial \hat{f} / \partial s$ is the gradient of the \hat{f} output w.r.t input feature, which follows θ^* . As the sampling function s is in

discrete space, Eq. (7) is not calculable, we need a proxy sampling function \hat{s} that satisfies the fundamental conditions: ▶ Differentiable; ▶ Approximate discrete sampling s with unbiased relaxation. Hence, the gradients may be approximated:

$$\nabla_{\alpha}\psi \approx \frac{\partial \hat{f}}{\partial \hat{s}} \cdot \frac{\partial \hat{s}}{\partial \alpha}, \quad \nabla_{\beta}\psi \approx \frac{\partial \hat{f}}{\partial \hat{s}} \cdot \frac{\partial \hat{s}}{\partial \beta}, \quad (8)$$

We treat these as the proxy gradients of the objective function w.r.t (α, β) .

We use the re-parameterize trick to realize \hat{s} . Concretely, operation feature \hat{s}_o are drawn from the Gumbel softmax distribution (Jang et al., 2017), for node i :

$$\hat{s}_o^{(i,j)} = \frac{\exp((\alpha^{(i,j)} + g^{(i,j)})/\tau)}{\sum_{m=0}^{M-1} \exp((\alpha^{(i,m)} + g^{(i,m)})/\tau)}, \quad (9)$$

where $0 \leq i < N - 1$, $0 \leq j < M - 1$, and $g^{(i,j)}$ are i.i.d samples drawn from Gumbel(0, 1), τ is the temperature within $[0, \infty)$. The $\alpha^{(i,j)}$ stands for the unnormalized-logit probability value of the candidate operation j at node i . Further, for topological structure samples \hat{s}_t :

$$\hat{s}_t^{(h,k)} = \sigma\left(\left(\beta^{(h,k)} + g^{(h,k)}\right)/\tau\right), \quad (10)$$

where $g^{(h,k)}$ are i.i.d samples drawn from Gumbel(0, 1) for $0 \leq h, k < N - 1$, and σ is the sigmoid function, which maps input to range (0, 1). The $\beta^{(h,k)}$ represents the log-odds value of the implicit probability variable $\gamma^{(h,k)}$, that is, $\beta^{(h,k)} = \log(\gamma^{(h,k)}/(1 - \gamma^{(h,k)}))$, $\gamma^{(h,k)} \in [0, 1]$.

We present the optimization proxy based search pseudocode as 1. Given the ideal proxy model \hat{f}_{θ^*} , for one search epoch, the proxy model iteratively takes the output of **Proxy sampling** function (\hat{s}) as input, it then undergoes the **Forward** pass, and directly takes model output as the maximization item for **Gradients calculation**. Subsequently, (α, β) are updated by **Gradients applied**, which are alternatively carried out over the predefined intervals, respectively. Finally, after optimization of specific epochs, the promising architecture batch **Sampling** based on currently optimized (α^*, β^*) are taken as search algorithm output.

2.3. Design Intentions and Analysis

As aforementioned, we explicitly propose two sets of proximal relationships: $\hat{f} \iff f$, $\hat{s} \iff s$, which derive four sets of proximal relationships: $\partial \hat{f} / \partial s \iff \partial f / \partial s$, $\partial \hat{f} / \partial \hat{s} \iff \partial \hat{f} / \partial s$, $\partial \hat{s} / \partial \alpha \iff \partial s / \partial \alpha$, $\partial \hat{s} / \partial \beta \iff \partial s / \partial \beta$. We present the design intentions in Figure 2. The discrete sampling and model fitting (\hat{f} approaching to f) implicitly establish the original gradients, as Eq. (7), but renders the propagation path non-differentiable. With the design of \hat{s} , we approximately achieve the full-path differentiable propagation. The analysis is summarized as follows:

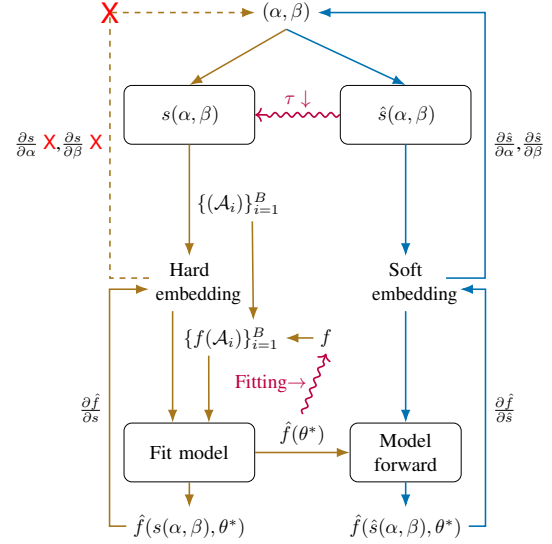


Figure 2: Illustration of the differentiable search strategy. The discrete sampling s renders the path non-differentiable. With the introduction of proxy sampling \hat{s} , it makes the propagation differentiable.

Algorithm 2 OptiProxy-NAS framework

- 1: **Input:** (α, β) , Proxy model \hat{f}_{θ} ;
- 2: **Parameters:** Evaluation function f ; Maximum evaluation number C ; Sampling number Q and the evaluation number B of each step;
- 3: **Output:** The optimal \mathcal{A}^* ;
- 4: $\mathcal{D} \leftarrow$ Randomly sample several architectures;
- 5: **while** $n \leq C$ **do**
- 6: Train the model \hat{f}_{θ} using \mathcal{D} ; ▶ Fitting
- 7: Search $\{\mathcal{A}_b\}_{b=1}^Q$ by Algorithm. 1(α, β); ▶ Search
- 8: Select $\{\mathcal{A}_b\}_{b=1}^B$ from $\{\mathcal{A}_b\}_{b=1}^Q$ by \hat{f}_{θ^*} ; ▶ Selection
- 9: Evaluate (query) the selected batch; ▶ Evaluation
- 10: $\mathcal{D} \leftarrow \mathcal{D} \cup \{(\mathcal{A}_b, f(\mathcal{A}_b))\}_{b=1}^B$; ▶ Dataset update
- 11: $n \leftarrow n + B$;
- 12: **end while**
- 13: $\mathcal{A}^* \leftarrow$ The historical best architecture in \mathcal{D} .

- Unbias: For the operations feature variable, in (Maddison et al., 2017), it has been proved that:

$$p\left(\lim_{\tau \rightarrow 0} \hat{s}_o^{(i,j)} = 1\right) = \text{softmax}(\alpha^i)^j, \quad (11)$$

which is the categorical variables in Eq. (5). In terms of topological structure variables, it also have been proved that:

$$p\left(\lim_{\tau \rightarrow 0} \hat{s}_t^{(h,k)} = 1\right) = \gamma^{(h,k)}, \quad (12)$$

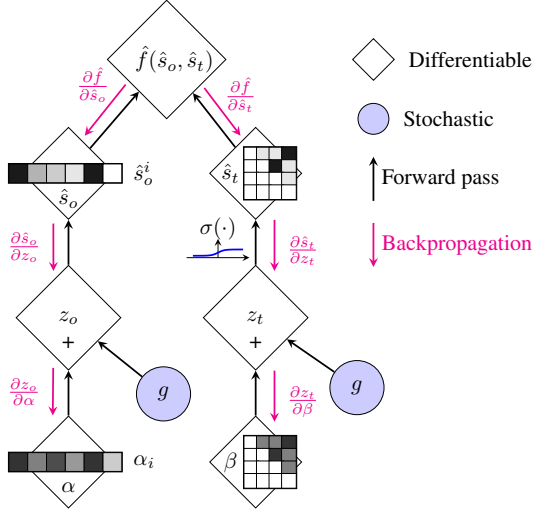


Figure 3: Gradient calculation in the computation graph.

which is the Bernoulli distribution variables in Eq. (6). We present these detailed proofs in Appendix A.5. Upon this, as $\tau \rightarrow 0$, then $\hat{s} \rightarrow s$, and then:

$$\frac{\partial \hat{f}}{\partial \hat{s}} \cdot \frac{\partial \hat{s}}{\partial \alpha} \rightarrow \frac{\partial \hat{f}}{\partial s} \cdot \frac{\partial s}{\partial \alpha}, \quad \frac{\partial \hat{f}}{\partial \hat{s}} \cdot \frac{\partial \hat{s}}{\partial \beta} \rightarrow \frac{\partial \hat{f}}{\partial s} \cdot \frac{\partial s}{\partial \beta}, \quad (13)$$

which makes the relaxation unbiased and enables the proxy gradients to approximate the original gradients.

- **Differentiable:** As in Figure 3, the re-parameterization allows gradients to flow from \hat{f} output to both α and β , to obtain the proxy gradients.
- **Unconstrained:** The optimization of continuous variables proceeds without constraint, that is, $\alpha \in \mathbb{R}^{N \times M}$, $\beta \in \mathbb{R}^{N \times N}$.
- **Exploration-exploitation dilemma:** The \mathcal{A}_o sampling by Eq.(5) and \mathcal{A}_t sampling by Eq.(6) introduce both exploration and exploitation. In the re-parameterization, the Gumbel noise variable g introduces randomness to (α, β) , facilitating exploration. During the early stages of search, a large τ encourages exploration, while in the later stages, as $\tau \rightarrow 0$, it facilitates exploitation.

2.4. Architecture Search Framework

Here we apply the sequential model based optimization (SMBO) as the main search framework. The pseudocode of our search framework is given in 2, the search begins with a randomly initialized dataset \mathcal{D} , iteratively undergoing *Model Fitting, Search, Selection, Evaluation, and Dataset Update*, as one search step. As \mathcal{D} is iteratively updated with newly evaluated architecture that undergoes optimization proxy based *search* and proxy model based *selection*, the fitting

of proxy model gradually achieves the better representation of the high-performance architecture regions. The iterative process continues for specific query cost constraints, to achieve the best historically evaluated architecture as the NAS result. The schematic of OptiProxy-NAS is presented in the Appendix A.3. Typically, an effective exploration strategy to avoid traps in local optima is crucial amidst a vast and potentially noisy space landscape. We have $\alpha = [\alpha_1, \alpha_2, \dots, \alpha_K]$ and $\beta = [\beta_1, \beta_2, \dots, \beta_K]$ denote the batches of parameters, where each α_i and β_i are initialized using Latin Hypercube Sampling (LHS). In one search step, considering Q candidate architectures, we sample Q/K architectures from each (α_i, β_i) group. This strategy attempts to enhance the sampling diversity and prevents the clustering in specific regions, which facilitates a systematic exploration. Fortunately, different groups of (α_i, β_i) share the query metrics and the proxy model, making it almost zero additional cost.

2.5. Proxy Model and Encoding Scheme

In theory, any differentiable model, not limited to the type and structure, combined with the corresponding architecture encoding scheme can work in OptiProxy-NAS framework. In this paper, we adopt a preliminary graph structure encoding scheme that treats candidate operations as nodes and feature maps as edges. The model takes the original one-hot feature matrix and one-hot adjacency matrix as inputs (White et al., 2020). A detailed explanation of encoding schemes for the search spaces is provided in Appendix A.8.

3. Experimental Results

To validate the effectiveness of OptiProxy-NAS, we follow the NAS best practice (see Appendix A.1) to set a fair empirical study. We choose 15 SOTA algorithms focusing on sample efficiency under the mainstream search strategies for comparison (see detailed experiment setup in Appendix A.7). To demonstrate the compatibility, we conduct preliminary experiments with MLP, LSTM and GAT. In particular, we report the comparison results based on the graph convolutional network (GCN) proposed by (Wen et al., 2020) (see details in Appendix A.4).

3.1. Tabular and Surrogate NAS Benchmarks

We first report the comparison results on four tabular and surrogate benchmarks.

NAS-Bench-201. Table 1 presents the comparison results of OptiProxy-NAS against the other 11 peer algorithms on the NAS-Bench-201 benchmark. Specifically, for the CIFAR-10 and CIFAR-100 datasets, OptiProxy-NAS obtains the reported optimum architecture with only 100 queries. Although DiNAS and AG-Net also find the optimum, they cost $2\times$ and $4\times$ more queries, respectively.

OptiProxy-NAS: Optimization Proxy based End-to-End Neural Architecture Search

Table 1: Comparison of results on NAS-Bench-201 cross different datasets. We search on `val` accuracy and report the mean±standard deviation result over 10 runs of different random seeds and the query number from the benchmark.

Method	CIFAR-10		CIFAR-100		ImageNet16-120		Queries	
	Val (%)	Test (%)	Val (%)	Test (%)	Val (%)	Test (%)		
Optimum*	91.61	94.37	73.49	73.51	46.77	47.31	–	
SGNAS (Huang & Chu, 2021)	90.18	93.53	70.28	70.31	44.65	44.98	–	
BANANAS†(White et al., 2021a)	91.56	94.30	73.49*	73.50	46.65	46.51	192	
Bayesian Opt. † (Snoek et al., 2015)	91.54	94.22	73.26	73.22	46.43	46.40	192	
Random Search † (Li & Talwalkar, 2019)	91.12	93.89	72.08	72.07	45.97	45.98	192	
GA-NAS (Rezaei et al., 2021)	–	94.34	–	73.28	–	46.80*‡	444	
MetaD2A (Lee et al., 2021)	94.37	94.38	73.34	73.34	–	–	500	
β-DARTS (Ye et al., 2022)	91.55	94.36	73.49*	73.51*	46.37	46.34	–	
TNAS (Shala et al., 2023)	–	94.37*	–	73.51*	–	–	–	
DiffusionNAG (An et al., 2023)	–	94.37*	–	73.51	–	–	–	
DiNAS (Asthana et al., 2024)	91.61*	94.37*	73.49*	73.51*	46.66	45.41	192	
AG-Net (Lukasik et al., 2022)	≈ 2× queries	91.41	94.16	73.14	73.15	46.42	46.43	100
		91.60	94.37*	73.49*	73.51*	46.64	46.43	192
		91.61*	94.37*	73.49*	73.51*	46.73	46.42	400
OptiProxy-NAS (Ours)	4× queries	91.61*	94.37*	73.49*	73.51*	46.64 ± 0.12	45.98‡	Reach "*" 100
		–	–	–	–	46.69 ± 0.1	45.79‡	even with 192
		–	–	–	–	46.77*	45.47‡	70% queries 280*

†: Results taken from (Lukasik et al., 2022). ‡: Following other works, we search on `val` accuracy to derive the optimal architecture and report its corresponding `test` accuracy. This metric (`test`) should not serve as an indicator of search performance.

Table 2: Comparison results on NB101, NB301 and NBNLP. We search on `val` accuracy and report the mean±standard deviation results over 10 runs with different random seeds.

Method	NAS-Bench-101			NAS-Bench-301		NAS-Bench-NLP	
	Val (%)	Test (%)	Queries	Val (%)	Queries	Val (%)	Queries
Optimum*	95.06	94.32	–	–	–	–	–
Arch2vec+RL (Yan et al., 2020)	–	94.10	400	–	–	–	–
Arch2vec+BO (Yan et al., 2020)	–	94.05	400	–	–	–	–
NAO † (Luo et al., 2018)	94.66	93.49	192	–	–	–	–
Random Search † (Li & Talwalkar, 2019)	94.31	93.61	192	94.31	195	95.64	304
Regularized Evolution † (Real et al., 2019)	94.47	93.89	192	94.75	192	95.66	304
BANANAS † (White et al., 2021a)	94.73	94.09	192	94.47	192	95.68	304
Local Search † (White et al., 2021b)	94.57	93.97	192	–	–	–	–
WeakNAS (Wu et al., 2021)	–	94.18	200	–	–	–	–
DiNAS (Asthana et al., 2024)	94.98	94.27	150	94.92	100	96.06	304
AG-Net (Lukasik et al., 2022)	94.90	94.18	192	94.79	192	95.95	304
OptiProxy-NAS (Ours)	94.98 ± 0.16	94.18‡	142	94.97 ± 0.05	100	96.18 ± 0.20	150
	–	–	–	94.81 ± 0.07	50	96.08 ± 0.19	75

†: Results taken from (Lukasik et al., 2022). ‡: The global optimal 95.06 (`val` accuracy) arch’s corresponding `test` accuracy is 94.23, we reach the optimum* over 8/10 of all seeds. We search on `val` accuracy, as stated, `test` metric does not represent the efficacy.

From a visual diagnostic analysis of the space and its exploration paths in Figure 4 of CIFAR-10 in Appendix A.7.3, we find that sampling based on (α, β) is rapidly guided to the high-performance region, significantly enhancing the overall sampling efficiency. We believe such improvement is bene-

fited from the proxy representation of the NAS space and gradient-based optimizer. For ImageNet16-120, the model scale setting in NAS-Bench-201 results in a relatively aggravated task difficulty and distribution complexity, making the space landscape appear noisier, which poses challenges

Table 3: Comparison results on HW-NAS-Bench. We report the mean results over 10 runs with different random seeds.

Device	Constraint	OptiProxy-NAS		AG-Net DiNAS		Optimum*
		200 (queries)	100 (50% fewer)	200 [†]	200 [‡]	
EdgeGPU	2	40.54 ± 0.19	40.12 ± 0.41	39.70	39.44	40.60
	4	44.56 ± 0.23	44.15 ± 0.63	42.80	43.91	44.80
	6	46.02 ± 0.23	45.65 ± 0.61	45.30	45.03	46.40
Raspi4	2	34.98 ± 0.22	34.91 ± 0.25	34.60	34.67	35.47
	4	43.36 ± 0.29	43.19 ± 0.32	42.00	43.25	43.63
	6	44.75 ± 0.39	44.69 ± 0.28	44.00	44.72	45.17
EdgeTPU	1	46.55 ± 0.11	46.52 ± 0.12	46.40	45.31	46.77
	2	41.10 ± 0.48	41.04 ± 0.49	40.90	40.01	41.30
Pixel3	4	45.86 ± 0.32	45.46 ± 0.48	45.30	44.74	45.97
	6	46.19 ± 0.29	45.97 ± 0.29	45.70	45.95	46.48
	6	46.19 ± 0.29	45.97 ± 0.29	45.70	45.95	46.48
Eyeris	1	45.03 ± 0.48	44.83 ± 0.10	44.50	44.67	45.16
FPGA	1	44.03 ± 0.19	43.85 ± 0.08	43.30	44.53 [‡]	44.37 [‡]

[†]: Results taken from (Asthana et al., 2024). [‡]: According to our tabular query, the optimum under constraint 1ms of FPGA is 44.37%.

for proxy representation and optimization. Theoretically, it is relatively hard to achieve a trade-off between query cost and performance on ImageNet16-120. Nevertheless, OptiProxy-NAS achieves the optimum with 280 queries, while no other peer algorithms have reported achieving this, e.g., AG-Net fails even with 400 queries. Compared to AG-Net, which costs at least 192 queries to obtain the near-optimal results (46.64), OptiProxy-NAS is more efficient as it costs $\approx 50\%$ fewer queries to reach the same results.

NAS-Bench-101. The search space of the NAS-Bench-101 benchmark is more challenging due to the existence of ‘isomorphic graphs’ and ‘validity constraints’, which introduce substantial optimization errors and perturbations when learning the topological structures and operation node features. Due to the page limit, detailed discussion upon the limitation and complexity is in Appendix A.8.2. The results in Table 2 also demonstrate the superiority of OptiProxy-NAS, which achieves the best of 94.98 ± 0.16 with 142 queries.

NAS-Bench-301 and NAS-Bench-NLP. For the surrogate benchmarks, NAS-Bench-301 (DARTS space) and NAS-Bench-NLP (RNN space). As Table 2 shows, the performance of OptiProxy-NAS is not only the best but also it costs much less queries (at least $4\times$ more efficient than the other 10 peer algorithms). This result is anticipated. Because these spaces are represented by surrogate models, they are relatively smoother and thus facilitating our proxy representation as well as the gradient-based end-to-end search. Additionally, to better demonstrate the effectiveness and stability throughout the search, we compare the performance of various methods in the best ever-sampled architecture over the query times. As in Figure 3 of Appendix A.7.2, OptiProxy-NAS shows superior results compared with the baseline methods, especially on NAS-Bench-301 and

Table 4: Comparison of total training epochs on NB201.

Setting	C10 (91.46)	C100 (73.49)	ImageNet (46.65)
OptiProxy-NAS	6000	20000	20000
OptiProxy-NAS (Low-fidelity)	3200	3500	7250

NAS-Bench-NLP.

3.2. Hardware-aware NAS Benchmark

To demonstrate the flexibility of OptiProxy-NAS, we further experiment on the resource-constrained NAS tasks of HW-NAS-Bench. To this end, we integrate an additional regression head into the proxy model to create a proxy representation of the search space spanning with architectures and latency metrics. In this unified optimization proxy, the proxy representations for these two cross-domain metrics share the architecture features but model the different landscape functions individually. Further, we use a weighted aggregation of the accuracy and latency as an evaluation metric. In particular, the weights are learnable based on the latency statistics of samples to provide latency constraint management. As shown in Table 3, across 6 of hardware devices (NN accelerators, edge and embedded devices), under 12 latency constraint settings, the performance of OptiProxy-NAS constantly outperforms the published best results. Significantly, we achieve better results than AG-Net in all 12 device latency settings, even with 50% fewer queries.

3.3. Low-fidelity Experiment

To assess the compatibility and flexibility, we conduct another experiment under a low-fidelity setting, where only 5 training epochs are allocated. We search for promising architectures batch using the low-fidelity metric and subsequently evaluate them with the high-fidelity metric to identify the best one. As shown in Figure 4, compared with the full training accuracy based search, the low-fidelity accuracy based search can achieve satisfying results within a limited number of total training epochs. For CIFAR-10, with an increase in the total epochs, the full training search gradually performs better due to the unbiased evaluation. For CIFAR-100 and ImageNet16-120, the low-fidelity search is consistently better than the full training search. We present the comparison results of total training epochs between low-fidelity search and full training search on NAS-Bench-201 in Table 4. To reach the same mean val accuracy, the low-fidelity search demonstrates a significant efficiency advantage.

3.4. Ablation Study

We conduct an ablation study regarding three design components of OptiProxy-NAS, i.e., (α, β) -based sampling, multi- (α, β) parallel exploration, and proxy model based

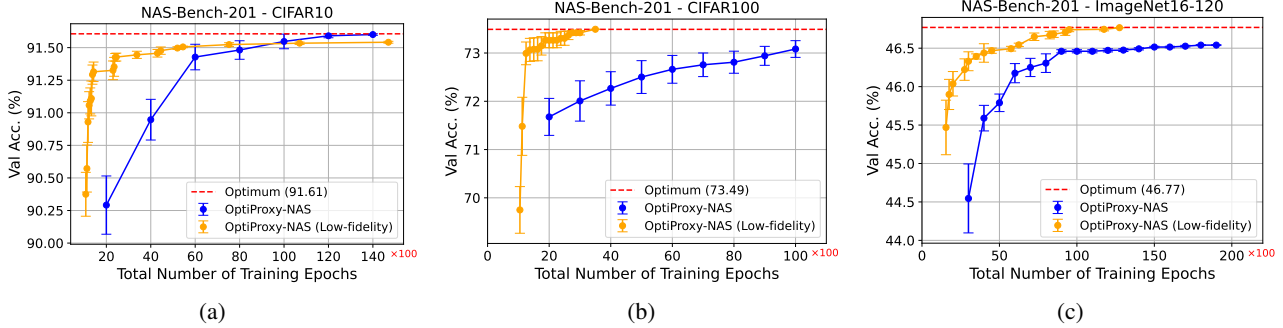


Figure 4: Comparison results of low-fidelity (5 epochs) search and full training (200 epochs) search (OptiProxy-NAS).

Table 5: Ablation study results. The query cost settings are 100/142/100/150 for NB201/NB101/NB301/NBNLP.

Method /Setting	No. of (α_i, β_i)	Selection	NB201			NB101	NB301	NBNLP
			C10	C100	ImageNet			
*	-	-	91.61	73.49	46.77	95.06	-	-
RS	-	-	91.12	72.08	45.97	94.31	94.31	95.64
S0	-	✗	91.08	69.56	45.65	94.55	94.33	95.80
S1	-	✓	91.51	72.91	46.30	94.59	94.66	95.90
S2	single	✗	91.54	72.30	45.93	94.69	94.64	95.79
S3	multi	✗	91.49	72.52	46.39	94.77	94.71	95.83
S4	single	✓	91.57	73.42	46.41	94.92	94.82	95.94
S5	multi	✓	91.61*	73.49*	46.64	94.98	94.97	96.18

selection. From the results in Table 5 (mean over 10-seeds runs), we confirm that all components are of importance. Specifically, (α, β) -based sampling is effective in resulting high-performance architectures. This results demonstrates that the selection can consolidate the reliability of our optimization proxy based search strategy and end-to-end search framework. In addition, we also notice that the multi- (α, β) parallel exploration strategy can improve the overall exploration, leading to better performance.

3.5. Resource and Time Cost

The additional cost of optimization proxy mainly comes from the training and backpropagation of the proxy model, which is highly compact (e.g., a two-layers GCN, 139.7K Parameters and 1.3MFLOPs), see details in Appendix A.4. The model’s complexity is $\mathcal{O}(N \times M \times K) + \mathcal{O}(N^2 \times K) + \mathcal{O}(N \times K^2)$, where N is the nodes number ($<$ dozens), M is the operation numbers ($<$ dozens), and K is the hidden neurons numbers, which does not scale with architecture or space. Experimentally, individually training 100 NB201-C10 architecture needs over 15 GPU-hours and 4GB of RAM. Our framework adds merely 20s and 10MB of additional memory, costing only 0.037% of runtime and 0.25% of memory.

4. Related Works

The individually sampling NAS (Zoph & Le, 2017; Sun et al., 2020) explore architectures within a discrete domain and generally rely on individual evaluation, which raises concerns about efficiency. Target this, predictor-guided sampling NAS employ proxy metrics (White et al., 2020; Wistuba & Pedapati, 2020; Yan et al., 2021) to provide quick evaluation (Dudziak et al., 2020; White et al., 2021a; Wei et al., 2023). In recent years, zero-cost metrics enable the NAS without requiring exhaustive training (Mellor et al., 2021; Abdelfattah et al., 2021), but they may also bias the search (White et al., 2022). In another way, the DARTS-series methods (Liu et al., 2019; Chen et al., 2019; Xie et al., 2019) relax the architecture space, by which to construct the supernet, then ensuring differentiable end-to-end search and weight-sharing based proxy evaluation. Inspired by generative models, some works reformulate NAS process as a generative paradigm, as seen in GA-NAS (Rezaei et al., 2021) and AG-Net (Lukasik et al., 2022). We provide additional details of related works in Appendix A.2.

5. Conclusion

This paper introduces a novel optimization proxy that redefines NAS as a differentiable optimization problem by employing a proxy representation of the search space, differentiable models, and relaxed architecture variables. Building on this foundation, we propose a differentiable search strategy that inherently balances exploration and exploitation. Furthermore, we introduce an end-to-end differentiable NAS framework (OptiProxy-NAS), streamlining the entire NAS process. Extensive experiments across 7 public benchmarks demonstrated it is effective, efficient, and flexible with real-world NAS metrics including platform-agnostic metrics, resource constraints and platform-specific metrics. In essence, OptiProxy-NAS is a general framework that can accommodate other search algorithms. We have experimentally used EA as the local search within it. For clarity, we opt to introduce the purely gradient-based

framework in this paper. We believe it paves a new avenue for NAS, and we hope it will serve as a foundation that revolves with and be complementary to recent research developments in multi-fidelity evaluation, learning curve extrapolation, weight-sharing evaluation, and zero-cost metrics. We use parallelization of (α, β) to promote diversity and tackle the isolated points. The (α_i, β_i) groups are optimized simultaneously, sharing metrics and optimization proxy. This also indicates the potential of parallelizing OptiProxy-NAS and we will explore this in future works.

Impact Statement

This paper presents work whose goal is to advance the field of Machine Learning. There are many potential societal consequences of our work, none which we feel must be specifically highlighted here.

References

- Abdelfattah, M. S., Mehrotra, A., Dudziak, L., and Lane, N. D. Zero-cost proxies for lightweight NAS. In *9th International Conference on Learning Representations, ICLR 2021, Virtual Event, Austria, May 3-7, 2021*. OpenReview.net, 2021.
- An, S., Lee, H., Jo, J., Lee, S., and Hwang, S. J. Diffusionag: Task-guided neural architecture generation with diffusion models. *CoRR*, abs/2305.16943, 2023.
- Asthana, R., Conrad, J., Dawoud, Y., Ortmanns, M., and Belagiannis, V. Multi-conditioned graph diffusion for neural architecture search. *CoRR*, abs/2403.06020, 2024.
- Baker, B., Gupta, O., Raskar, R., and Naik, N. Accelerating neural architecture search using performance prediction. In *6th International Conference on Learning Representations, ICLR 2018, Vancouver, BC, Canada, April 30 - May 3, 2018, Workshop Track Proceedings*. OpenReview.net, 2018.
- Brock, A., Lim, T., Ritchie, J. M., and Weston, N. Smash: one-shot model architecture search through hypernetworks. In *International Conference on Learning Representations, Vancouver, BC, Canada*, pp. 1–21, 2018a.
- Brock, A., Lim, T., Ritchie, J. M., and Weston, N. SMASH: one-shot model architecture search through hypernetworks. In *6th International Conference on Learning Representations, ICLR 2018, Vancouver, BC, Canada, April 30 - May 3, 2018, Conference Track Proceedings*. OpenReview.net, 2018b.
- Cai, H., Zhu, L., and Han, S. Proxylessnas: Direct neural architecture search on target task and hardware. In *7th International Conference on Learning Representations, ICLR 2019, New Orleans, LA, USA, May 6-9, 2019*. OpenReview.net, 2019.
- Chen, W., Park, S., Tanneau, M., and Hentenryck, P. V. Learning optimization proxies for large-scale security-constrained economic dispatch. *CoRR*, abs/2112.13469, 2021.
- Chen, W., Tanneau, M., and Hentenryck, P. V. End-to-end feasible optimization proxies for large-scale economic dispatch. *CoRR*, abs/2304.11726, 2023.
- Chen, X., Xie, L., Wu, J., and Tian, Q. Progressive differentiable architecture search: bridging the depth gap between search and evaluation. In *IEEE/CVF International Conference on Computer Vision, Seoul, Korea (South)*, pp. 1294–1303. IEEE, 2019.
- Dong, X. and Yang, Y. Nas-bench-201: Extending the scope of reproducible neural architecture search. In *8th International Conference on Learning Representations, ICLR 2020, Addis Ababa, Ethiopia, April 26-30, 2020*. OpenReview.net, 2020.
- Dudziak, L., Chau, T., Abdelfattah, M. S., Lee, R., Kim, H., and Lane, N. D. BRP-NAS: prediction-based NAS using gns. In Larochelle, H., Ranzato, M., Hadsell, R., Balcan, M., and Lin, H. (eds.), *Advances in Neural Information Processing Systems 33: Annual Conference on Neural Information Processing Systems 2020, NeurIPS 2020, December 6-12, 2020, virtual*, 2020.
- Elmachtoub, A. N. and Grigas, P. Smart “predict, then optimize”. *Manag. Sci.*, 68(1):9–26, 2022.
- Guo, Z., Zhang, X., Mu, H., Heng, W., Liu, Z., Wei, Y., and Sun, J. Single path one-shot neural architecture search with uniform sampling. In Vedaldi, A., Bischof, H., Brox, T., and Frahm, J. (eds.), *European Conference on Computer Vision, Glasgow, UK*, volume 12361 of *Lecture Notes in Computer Science*, pp. 544–560. Springer, 2020.
- Huang, S. and Chu, W. Searching by generating: Flexible and efficient one-shot NAS with architecture generator. In *IEEE Conference on Computer Vision and Pattern Recognition, CVPR 2021, virtual, June 19-25, 2021*, pp. 983–992. Computer Vision Foundation / IEEE, 2021.
- Jang, E., Gu, S., and Poole, B. Categorical reparameterization with gumbel-softmax. In *5th International Conference on Learning Representations, ICLR 2017, Toulon, France, April 24-26, 2017, Conference Track Proceedings*. OpenReview.net, 2017.
- Klyuchnikov, N., Trofimov, I., Artemova, E., Salnikov, M., Fedorov, M., Filippov, A., and Burnaev, E. Nas-bench-nlp: neural architecture search benchmark for natural

- language processing. *IEEE Access*, 10:45736–45747, 2022.
- Kotary, J., Vito, V. D., Christopher, J., Hentzenryck, P. V., and Fioretto, F. Predict-then-optimize by proxy: Learning joint models of prediction and optimization. *CoRR*, abs/2311.13087, 2023.
- Lee, H., Hyung, E., and Hwang, S. J. Rapid neural architecture search by learning to generate graphs from datasets. In *9th International Conference on Learning Representations, ICLR 2021, Virtual Event, Austria, May 3-7, 2021*. OpenReview.net, 2021.
- Li, C., Yu, Z., Fu, Y., Zhang, Y., Zhao, Y., You, H., Yu, Q., Wang, Y., Hao, C., and Lin, Y. Hw-nas-bench: Hardware-aware neural architecture search benchmark. In *9th International Conference on Learning Representations, ICLR 2021, Virtual Event, Austria, May 3-7, 2021*. OpenReview.net, 2021.
- Li, G., Qian, G., Delgado, I. C., Müller, M., Thabet, A. K., and Ghanem, B. SGAS: sequential greedy architecture search. In *2020 IEEE/CVF Conference on Computer Vision and Pattern Recognition, CVPR 2020, Seattle, WA, USA, June 13-19, 2020*, pp. 1617–1627. Computer Vision Foundation / IEEE, 2020.
- Li, L. and Talwalkar, A. Random search and reproducibility for neural architecture search. In Globerson, A. and Silva, R. (eds.), *Proceedings of the Thirty-Fifth Conference on Uncertainty in Artificial Intelligence, UAI 2019, Tel Aviv, Israel, July 22-25, 2019*, volume 115 of *Proceedings of Machine Learning Research*, pp. 367–377. AUAI Press, 2019.
- Liu, H., Simonyan, K., and Yang, Y. Darts: differentiable architecture search. In *International Conference on Learning Representations, New Orleans, LA, USA, pp. 1–11, 2019*.
- Lukasik, J., Jung, S., and Keuper, M. Learning where to look - generative NAS is surprisingly efficient. *CoRR*, abs/2203.08734, 2022.
- Luo, R., Tian, F., Qin, T., Chen, E., and Liu, T. Neural architecture optimization. In Bengio, S., Wallach, H. M., Larochelle, H., Grauman, K., Cesa-Bianchi, N., and Garnett, R. (eds.), *Advances in Neural Information Processing Systems 31: Annual Conference on Neural Information Processing Systems 2018, NeurIPS 2018, December 3-8, 2018, Montréal, Canada*, pp. 7827–7838, 2018.
- Maddison, C. J., Mnih, A., and Teh, Y. W. The concrete distribution: A continuous relaxation of discrete random variables. In *5th International Conference on Learning Representations, ICLR 2017, Toulon, France, April 24-26, 2017, Conference Track Proceedings*. OpenReview.net, 2017.
- Mellor, J., Turner, J., Storkey, A. J., and Crowley, E. J. Neural architecture search without training. In Meila, M. and Zhang, T. (eds.), *Proceedings of the 38th International Conference on Machine Learning, ICML 2021, 18-24 July 2021, Virtual Event*, volume 139 of *Proceedings of Machine Learning Research*, pp. 7588–7598. PMLR, 2021.
- Pham, H., Guan, M. Y., Zoph, B., Le, Q. V., and Dean, J. Efficient neural architecture search via parameter sharing. In Dy, J. G. and Krause, A. (eds.), *International Conference on Machine Learning, Stockholm, Sweden*, volume 80, pp. 4092–4101, 2018.
- Real, E., Aggarwal, A., Huang, Y., and Le, Q. V. Regularized evolution for image classifier architecture search. In *The Thirty-Third AAAI Conference on Artificial Intelligence, Honolulu, Hawaii, USA, pp. 4780–4789, 2019*.
- Rezaei, S. S. C., Han, F. X., Niu, D., Salameh, M., Mills, K. G., Lian, S., Lu, W., and Jui, S. Generative adversarial neural architecture search. In Zhou, Z. (ed.), *Proceedings of the Thirtieth International Joint Conference on Artificial Intelligence, IJCAI 2021, Virtual Event / Montreal, Canada, 19-27 August 2021*, pp. 2227–2234. ijcai.org, 2021.
- Rombach, R., Blattmann, A., Lorenz, D., Esser, P., and Ommer, B. High-resolution image synthesis with latent diffusion models. In *IEEE/CVF Conference on Computer Vision and Pattern Recognition, CVPR 2022, New Orleans, LA, USA, June 18-24, 2022*, pp. 10674–10685. IEEE, 2022.
- Shala, G., Elsken, T., Hutter, F., and Grabocka, J. Transfer NAS with meta-learned bayesian surrogates. In *The Eleventh International Conference on Learning Representations, ICLR 2023, Kigali, Rwanda, May 1-5, 2023*. OpenReview.net, 2023.
- Siems, J., Zimmer, L., Zela, A., Lukasik, J., Keuper, M., and Hutter, F. Nas-bench-301 and the case for surrogate benchmarks for neural architecture search. *CoRR*, abs/2008.09777, 2020.
- Snoek, J., Rippel, O., Swersky, K., Kiros, R., Satish, N., Sundaram, N., Patwary, M. M. A., Prabhakar, and Adams, R. P. Scalable bayesian optimization using deep neural networks. In Bach, F. R. and Blei, D. M. (eds.), *Proceedings of the 32nd International Conference on Machine Learning, ICML 2015, Lille, France, 6-11 July 2015*, volume 37 of *JMLR Workshop and Conference Proceedings*, pp. 2171–2180. JMLR.org, 2015.

- Sun, Y., Xue, B., Zhang, M., Yen, G. G., and Lv, J. Automatically designing cnn architectures using the genetic algorithm for image classification. *IEEE transactions on cybernetics*, 50(9):3840–3854, 2020.
- Wei, C., Niu, C., Tang, Y., Wang, Y., Hu, H., and Liang, J. NPENAS: neural predictor guided evolution for neural architecture search. *IEEE Trans. Neural Networks Learn. Syst.*, 34(11):8441–8455, 2023. doi: 10.1109/TNNLS.2022.3151160.
- Wen, W., Liu, H., Chen, Y., Li, H. H., Bender, G., and Kindermans, P. Neural predictor for neural architecture search. In Vedaldi, A., Bischof, H., Brox, T., and Frahm, J. (eds.), *European Conference on Computer Vision, Glasgow, UK*, volume 12374, pp. 660–676, 2020.
- White, C., Neiswanger, W., Nolen, S., and Savani, Y. A study on encodings for neural architecture search. In Larochelle, H., Ranzato, M., Hadsell, R., Balcan, M., and Lin, H. (eds.), *Advances in Neural Information Processing Systems 33: Annual Conference on Neural Information Processing Systems 2020, NeurIPS 2020, December 6-12, 2020, virtual*, pp. 1–13, 2020.
- White, C., Neiswanger, W., and Savani, Y. BANANAS: bayesian optimization with neural architectures for neural architecture search. In *Thirty-Fifth AAAI Conference on Artificial Intelligence, AAAI 2021*, pp. 10293–10301. AAAI Press, 2021a.
- White, C., Nolen, S., and Savani, Y. Exploring the loss landscape in neural architecture search. In de Campos, C. P., Maathuis, M. H., and Quaeghebeur, E. (eds.), *Proceedings of the Thirty-Seventh Conference on Uncertainty in Artificial Intelligence, UAI 2021, Virtual Event, 27-30 July 2021*, volume 161 of *Proceedings of Machine Learning Research*, pp. 654–664. AUAI Press, 2021b.
- White, C., Zela, A., Ru, R., Liu, Y., and Hutter, F. How powerful are performance predictors in neural architecture search? In Ranzato, M., Beygelzimer, A., Dauphin, Y. N., Liang, P., and Vaughan, J. W. (eds.), *Advances in Neural Information Processing Systems 34: Annual Conference on Neural Information Processing Systems 2021, NeurIPS 2021, December 6-14, 2021, virtual*, pp. 28454–28469, 2021c.
- White, C., Khodak, M., Tu, R., Shah, S., Bubeck, S., and Dey, D. A deeper look at zero-cost proxies for lightweight nas. In *ICLR Blog Track, 2022*. <https://iclr-blog-track.github.io/2022/03/25/zero-cost-proxies/>.
- White, C., Safari, M., Sukthanker, R., Ru, B., Elsken, T., Zela, A., Dey, D., and Hutter, F. Neural architecture search: Insights from 1000 papers. *CoRR*, abs/2301.08727, 2023.
- Wistuba, M. and Pedapati, T. Learning to rank learning curves. In *Proceedings of the 37th International Conference on Machine Learning, ICML 2020, 13-18 July 2020, Virtual Event*, volume 119 of *Proceedings of Machine Learning Research*, pp. 10303–10312. PMLR, 2020.
- Wu, J., Dai, X., Chen, D., Chen, Y., Liu, M., Yu, Y., Wang, Z., Liu, Z., Chen, M., and Yuan, L. Stronger NAS with weaker predictors. In Ranzato, M., Beygelzimer, A., Dauphin, Y. N., Liang, P., and Vaughan, J. W. (eds.), *Advances in Neural Information Processing Systems 34: Annual Conference on Neural Information Processing Systems 2021, NeurIPS 2021, December 6-14, 2021, virtual*, pp. 28904–28918, 2021.
- Xiao, H., Wang, Z., Zhu, Z., Zhou, J., and Lu, J. Shapley-nas: Discovering operation contribution for neural architecture search. In *IEEE/CVF Conference on Computer Vision and Pattern Recognition, CVPR 2022, New Orleans, LA, USA, June 18-24, 2022*, pp. 11882–11891. IEEE, 2022.
- Xie, L., Chen, X., Bi, K., Wei, L., Xu, Y., Wang, L., Chen, Z., Xiao, A., Chang, J., Zhang, X., et al. Weight-sharing neural architecture search: a battle to shrink the optimization gap. *ACM Computing Surveys*, 54(9):1–37, 2021.
- Xie, S., Zheng, H., Liu, C., and Lin, L. SNAS: stochastic neural architecture search. In *7th International Conference on Learning Representations, ICLR 2019, New Orleans, LA, USA, May 6-9, 2019*. OpenReview.net, 2019.
- Yan, S., Zheng, Y., Ao, W., Zeng, X., and Zhang, M. Does unsupervised architecture representation learning help neural architecture search? In Larochelle, H., Ranzato, M., Hadsell, R., Balcan, M., and Lin, H. (eds.), *Advances in Neural Information Processing Systems 33: Annual Conference on Neural Information Processing Systems 2020, NeurIPS 2020, December 6-12, 2020, virtual*, 2020.
- Yan, S., White, C., Savani, Y., and Hutter, F. Nas-bench-x11 and the power of learning curves. In Ranzato, M., Beygelzimer, A., Dauphin, Y. N., Liang, P., and Vaughan, J. W. (eds.), *Advances in Neural Information Processing Systems 34: Annual Conference on Neural Information Processing Systems 2021, NeurIPS 2021, December 6-14, 2021, virtual*, pp. 22534–22549, 2021.
- Ye, P., Li, B., Li, Y., Chen, T., Fan, J., and Ouyang, W. β -darts: Beta-decay regularization for differentiable architecture search. In *IEEE/CVF Conference on Computer Vision and Pattern Recognition, CVPR 2022, New Orleans, LA, USA, June 18-24, 2022*, pp. 10864–10873. IEEE, 2022.
- Ying, C., Klein, A., Christiansen, E., Real, E., Murphy, K., and Hutter, F. Nas-bench-101: towards reproducible

neural architecture search. In Chaudhuri, K. and Salakhutdinov, R. (eds.), *International Conference on Machine Learning, California, USA*, volume 97, pp. 7105–7114, 2019.

Yuan, E., Chen, W., and Hentenryck, P. V. Reinforcement learning from optimization proxy for ride-hailing vehicle relocation. *J. Artif. Intell. Res.*, 75:985–1002, 2022.

Zela, A., Elsken, T., Saikia, T., Marrakchi, Y., Brox, T., and Hutter, F. Understanding and robustifying differentiable architecture search. In *International Conference on Learning Representations, Addis, Ethiopia*, pp. 1–11. OpenReview.net, 2020.

Zhou, D., Zhou, X., Zhang, W., Loy, C. C., Yi, S., Zhang, X., and Ouyang, W. Econas: Finding proxies for economical neural architecture search. In *2020 IEEE/CVF Conference on Computer Vision and Pattern Recognition, CVPR 2020, Seattle, WA, USA, June 13-19, 2020*, pp. 11393–11401. Computer Vision Foundation / IEEE, 2020.

Zoph, B. and Le, Q. V. Neural architecture search with reinforcement learning. In *International Conference on Learning Representations, Toulon, France*, pp. 1–16, 2017.

Zoph, B., Vasudevan, V., Shlens, J., and Le, Q. V. Learning transferable architectures for scalable image recognition. In *Proceedings of the IEEE conference on computer vision and pattern recognition*, pp. 8697–8710, 2018.

A. Appendix

A.1. The NAS Best Practices Checklist

A.1.1. BEST PRACTICES FOR RELEASING CODE

For all experiments you report, check if you released:

- Code for the training pipeline used to evaluate the final architectures. [N/A], for fair comparison, this work regards the popular benchmarks: NAS-Bench-101, NAS-Bench-201, NAS-Bench-301, NAS-Bench-NLP, HW-NAS-Bench. The training pipelines for evaluation are released in their original repositories.
- Code for the search space. [N/A].
- The hyperparameters used for the final evaluation pipeline, as well as random seeds [N/A].
- Code for your NAS method. [Yes], we will release our NAS framework code.
- Hyperparameters for your NAS method, as well as random seeds. [Yes], we will release our hyperparameter settings, as well as the random seeds.

Note that the easiest way to satisfy the first three of these is to use existing NAS benchmarks, rather than changing them or introducing new ones. [Yes], we fully agree with and comply with this practice item, to structure this work.

A.1.2. BEST PRACTICES FOR COMPARING NAS METHODS

- For all NAS methods you compare, did you use exactly the same NAS benchmark, including the same dataset (with the same training-test split), search space and code for training the architectures and hyperparameters for that code? [Yes], this work regards the popular benchmarks: NAS-Bench-101, NAS-Bench-201, NAS-Bench-301, NAS-Bench-NLP, HW-NAS-Bench. The dataset, training-test split, search space, code for training and hyperparameters are exactly the same for fair comparison.
- Did you control for confounding factors (different hardware, versions of DL libraries, different runtimes for the different methods)? [Yes], we use the same environment setting for all benchmark experiments, but running on GPU/CPU, or combined to implement the search pipeline, there exists a subtle bias on the final results.
- Did you run ablation studies? [Yes], we ran a thorough ablation study.
- Did you use the same evaluation protocol for the methods being compared? [Yes].

Did you compare performance over time? [N/A], we run experiments on 7 benchmarks for fair comparison and to compare performance over query numbers. Note that the number of queries is almost perfectly correlated with runtime.

Did you compare to random search? [Yes].

Did you perform multiple runs of your experiments and report seeds? [Yes], We ran 10 trials across all benchmarks and datasets, reporting the mean value, also with standard derivation.

Did you use tabular or surrogate benchmarks for in-depth evaluations? [Yes], both.

A.1.3. BEST PRACTICES FOR REPORTING IMPORTANT DETAILS

Did you report how you tuned hyperparameters, and what time and resources this required? [Yes], in the Appendix Section A.9.1.

Did you report the time for the entire end-to-end NAS method (rather than, e.g., only for the search phase)? [N/A], we run experiments on 7 benchmarks for fair comparison and to compare performance over query numbers. We do not target the evaluation acceleration strategies but have demonstrated promising results in low-fidelity experiments. Note that the number of queries is almost perfectly correlated with runtime.

Did you report all the details of your experimental setup? [Yes], we reported all details of our experimental setup in Appendix Section A.7.1.

A.2. Related works

Predictor-guided sampling NAS. Individually heuristic NAS methods formulate the search as the “black box” optimization problem. Typical methods utilize Evolutionary Algorithms (EA) (Sun et al., 2020), Reinforcement Learning (RL) (Zoph & Le, 2017; Zoph et al., 2018), Bayesian Optimization (BO) (White et al., 2021a), and Local Search (LS) (White et al., 2021b) methods as the exploration strategies. Overall, the individually heuristic NAS methods explore architectures within a discrete domain and generally rely on individual evaluation, which raises concerns about efficiency. Target this, predictor-based NAS employ surrogate models as predictors along with encoding schemes (White et al., 2020; Yan et al., 2021; Wistuba & Pedapati, 2020; Baker et al., 2018) to provide quick evaluation to the optimizer or sampling process. Notable works include NPENAS (Wei et al., 2023), BANANAS (White et al., 2021a) and BRP-NAS (Dudziak et al., 2020). Zero-cost metrics also play a crucial role in assisting the optimizer as the predictor

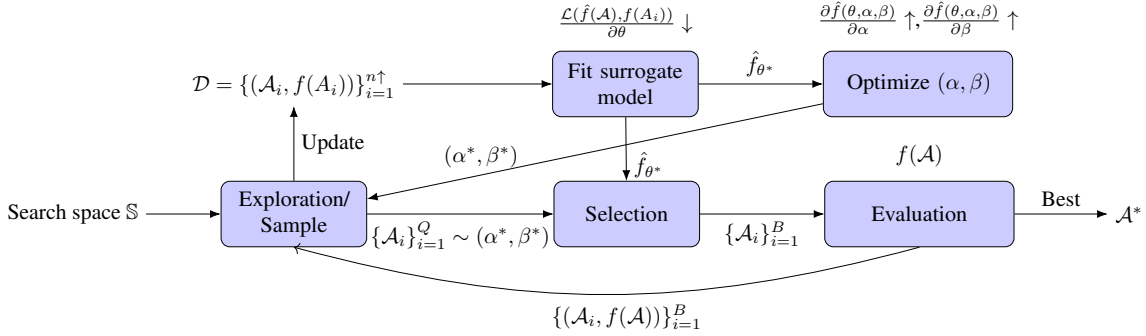


Figure 1: Framework for Optimization Proxy based end-to-end Neural Architecture Search (OptiProxy-NAS).

without requiring exhaustive training. The fundamental principle is to leverage saliency criteria, e.g., Fisher, Grad Norm, Grasp, Jac. Cov., SynFlow, SNIP (Mellor et al., 2021; Abdelfattah et al., 2021). However, according to the empirical study of (White et al., 2022), the nature of unreliable performance, harmful biases, and inconsistent performance across tasks of zero-cost metrics may have strong preferences that may bias the search, especially the data-agnostic proxies. OptiProxy-NAS focuses on improving search efficiency, it operates entirely in parallel with existing EA, RL, and BO approaches, yet is theoretically orthogonal and compatible with existing proxy models and zero-cost metrics.

Weight-sharing NAS. From another perspective, to address the evaluation-expensive issue, several studies (Pham et al., 2018; Brock et al., 2018a; Zela et al., 2020; Guo et al., 2020) introduce the weight-sharing evaluation strategy by constructing a unified hypernetwork, from which sub-architectures shared the weights. Additionally, the DARTS-series methods (Liu et al., 2019; Chen et al., 2019; Li et al., 2020; Xie et al., 2019; Xiao et al., 2022) relax the architecture space, then optimize both the architecture parameters and supernet weights through gradient descent, significantly enhancing the efficiency of the search and evaluation. OptiProxy-NAS does not involve training acceleration strategies, in principle, they are orthogonal and compatible with our framework. We also draw on the concept of reparameterization trick to reach the unbiased relaxation of the discrete architecture space in SNAS (Xie et al., 2019), however, not for the parameters learning of architectural weights in supernet, but for the relaxed architecture variable.

Generative NAS. Inspired by the advancements of generative models, it offers a new perspective on reformulating the NAS problem, transforming the sampling-and-validation optimization process into a generative one, e.g., GA-NAS (Rezaei et al., 2021) AG-Net (Lukasik et al., 2022), DiffusionNAG (An et al., 2023). Especially, DiNAS (Asthana et al., 2024) achieves the current state-of-the-art results across nearly almost NAS benchmarks. In-

spired by diffusion models (Rombach et al., 2022) on visual generation tasks, DiffusionNAG (An et al., 2023) employs a diffusion model for their generation. The predictor-guided mechanism in DiffusionNAG enables the generation of task-specific optimal architectures by sampling from regions likely to exhibit desired properties. DiNAS (Asthana et al., 2024) introduces a graph diffusion-based NAS method, utilizing discrete conditional diffusion processes to generate high-performing architectures.

Optimization proxy. As the proceeded of this work, we became aware of similar concepts of ‘‘Smart Predict-Then-Optimize’’ (Elmachtoub & Grigas, 2022), being applied to traditional optimization problems. Additionally, optimization proxies, particularly those based on deep neural networks, are designed to reduce the computational load of traditional solvers by directly predicting optimal or near-optimal solutions (Kotary et al., 2023). Common application scenarios include reinforcement learning in decision-making problems (Yuan et al., 2022) and large-scale economic dispatch problems (Chen et al., 2023). Independently conceived, we bring up this similar concept to formulate the NAS as a gradient-based ‘‘End-to-end Predict-then-Optimize’’ framework.

A.3. Search framework

For clarity and clear comparison with related works, we additionally present the schematic of the pipeline of OptiProxy-NAS framework in Figure 1.

A.4. Proxy models

We provide a detailed description of the GCN model, which we employ as the proxy model in our preliminary experiments. The initialization of each node in the graph begins with a D_0 -dimensional representation, providing an initial feature vector $V_0 \in \mathbb{R}^{N \times M}$, which is the one-hot vector to indicate the operation choice. The adjacency matrix $A \in \mathbb{R}^{N \times N}$ represents the node connections, For each propagation layer l , a learnable weight matrix is as

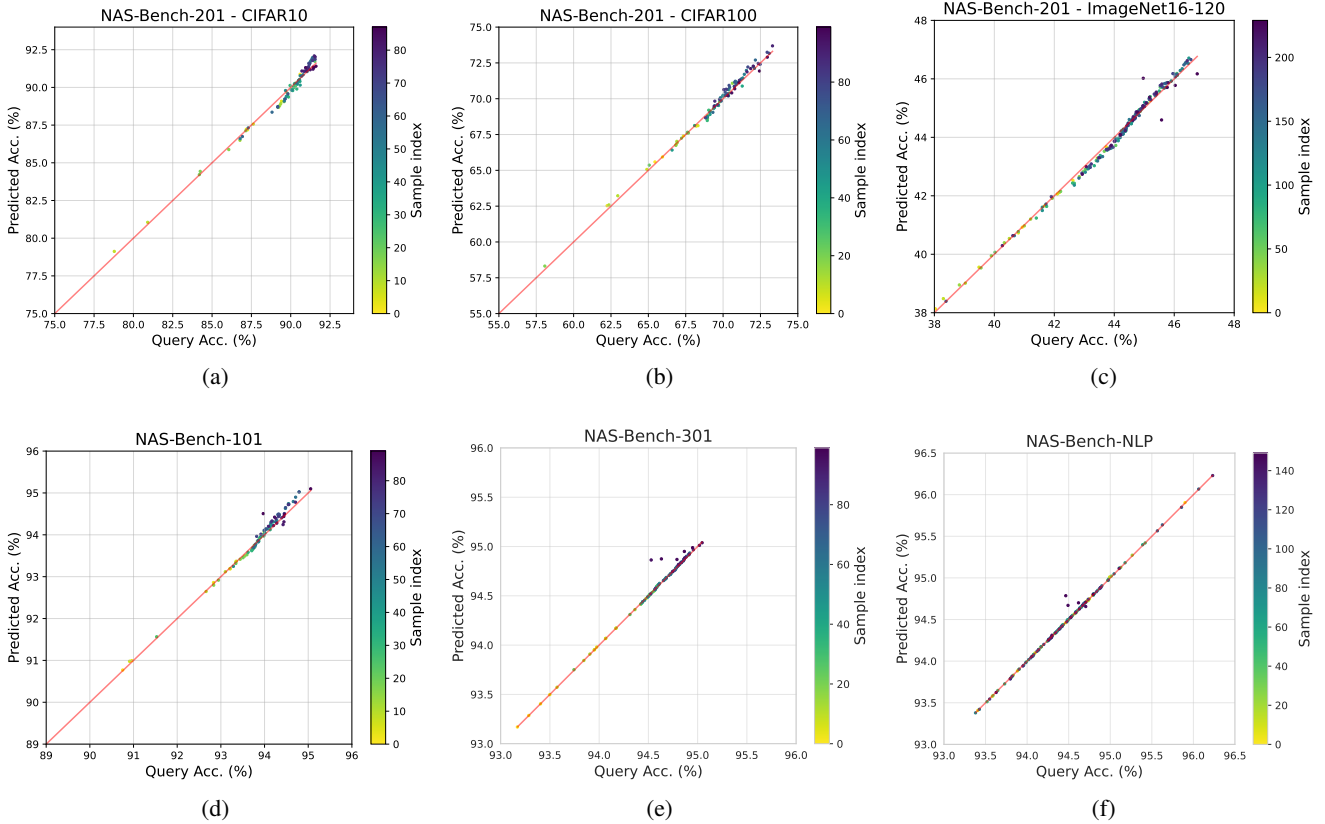


Figure 2: The scatter of the evaluated architectures. We distinguish the sampling order of the architecture points by coloring them.

$W_l \in \mathbb{R}^{D_l \times D_{l+1}}$, and layer-wise propagation as follows:

$$V_{l+1} = \text{ReLU}(AV_l W_l). \quad (1)$$

The prior predictor-based NAS study (Wen et al., 2020) employs the `average` operation over the bidirectional information propagation. One direction propagates information using A and another direction by A^T , follows:

$$V_{l+1} = 1/2 * \text{ReLU}(AV_l W_l^+) + 1/2 * \text{ReLU}(A^T V_l W_l^-) \quad (2)$$

Alternatively, we use the `concatenation` followed by a linear layer to preserve the information from both directions. Further, we add layer normalization to keep variables within a proper range and `GeLU` activation for better nonlinearity in the fully connected layer:

$$V_{l+1} = \mathcal{LN}(\text{Linear}(\text{concat}(\text{GeLU}(AV_l W_l) + \text{GeLU}(A^T V_l W_l)))) \quad (3)$$

We employ the weighted combination of the Mean Squared Error (MSE) loss and the pairwise ranking loss, as:

$$\mathcal{L} = \mathcal{L}_{mse} + \lambda \mathcal{L}_{rank}, \quad (4)$$

where λ is the ranking loss weight coefficient, and:

$$\mathcal{L}_{rank}(\{(\mathcal{A}_j, y_j)\}_{j=1, \dots, N}) = \sum_{j=1}^N \sum_{\{i, j | y_i > y_j\}} \max(0, m - (\hat{f}(\mathcal{A}_i) - \hat{f}(\mathcal{A}_j))). \quad (5)$$

where m is the margin, and y_i is the ground truth accuracy of \mathcal{A}_i , this ranking loss emphasizes the relative ordering of predicted values rather than their absolute magnitudes. During the sampling process of our experiments, we monitor and record the distribution of model predictions and ground-truth values for the sampled and evaluated architectures. As shown in Figure 2, it not only demonstrates the model’s representation of the space landscape but also roughly illustrates the sampling process and convergence trend. Theoretically, our framework is compatible with most gradient-based models. We conduct the experiment with MLP, LSTM, and GAT on NAS-Bench-201, with results available in Table 1. Since these are merely preliminary experiments, similar to the GCN model, we only employ the original encoding scheme, and stretch or serialize the \mathcal{A}_t and \mathcal{A}_o to adapt to different proxy models. Therefore,

the experiments on these models are not comprehensive and in-depth.

Table 1: Preliminary experiments of different models on NAS-Bench-201 under 100 query times over 10 seeds (0 ~ 9).

Model	CIFAR-10	CIFAR-100	ImageNet16-120
Optimum*	91.61	73.49	46.77
GCN	91.61	73.49	46.64
MLP	91.61	73.49	46.61
LSTM	91.14	70.51	46.07
GAT	91.44	72.91	45.81

A.5. Proofs of relaxation unbiased

Before providing the proofs, we first reiterate the design intention of our search algorithm to ensure clarity. Here we elaborate our rationale from these aspects:

- Design Intention:** The Bernoulli distribution in Eq. (6) models the probability of connections between operations, enabling a continuous relaxation of the topological space. Although the assumption of edge independence simplifies the model, our experiments demonstrate that the proxy model effectively captures interactions or joint probability distributions between edges, enhancing the representation capability of our “optimization proxy”.
- Design Benefits:** This approach simplifies the representation of binary decisions (i.e., whether connections exist or not). For each edge, only one parameter (i.e., the continuous probability p) needs to be optimized using gradient-based methods.
- Co-design of Sampling and Proxy Sampling:**

For node features, the proxy sampling based on Eq. (5) aligns with the discrete sampling of Eq. (9) in the main paper part.

For topological features, the proxy sampling based on Eq. (6) aligns with the discrete sampling of Eq. (10) in the main paper part.
- Consistent Mathematical Form:** The Bernoulli distribution is a special case of the categorical distribution for two outcomes, ensuring consistency in the mathematical form across related functions.

We present the proof of unbiased relaxation in operation node propagation in Eq. (11) of the main paper part. For clarity, we omit the node index i , consider a specific feature node, and denote the operation index j as the subscript, we

denote Eq. (11) in the main part as:

$$\hat{s}_o(\alpha)_j = \frac{\exp((\alpha_j + g_j)/\tau)}{\sum_{m=1}^M \exp((\alpha_m + g_m)/\tau)}, \quad (6)$$

where $0 \leq j < M$, and τ is the temperature. α_j is the unnormalized-logit of probability of the candidate operation choice. Further, g follows Gumbel distribution, i.e., $g = -\log(-\log(u))$, where $u \sim \text{Uniform}(0, 1)$. Additionally, we have $\alpha = \log(\pi)$, where $\pi \in (0, \infty)$. It has been proved in (Maddison et al., 2017) that:

$$\begin{aligned} \mathbb{P}\left(\lim_{\tau \rightarrow 0} \hat{s}_o(\alpha)_j = 1\right) &= \pi_j / \sum_{m=1}^M \pi_m = e^{\alpha_j} / \sum_{m=1}^M e^{\alpha_m} \\ &= \text{softmax}(\alpha)_j, \end{aligned} \quad (7)$$

which is the categorical distribution in Eq. (5) in the main body of this paper.

For the unbiased relaxation in topological structure propagation, as Eq. (12) of the main paper part. We also omit the connection index (h, k) , i.e., considering a specific connection between two nodes, the Eq. (12) of the main paper part expressed as:

$$\begin{aligned} \hat{s}_t(\beta) &= \sigma((\beta + g)/\tau) \\ &= \frac{1}{1 + \exp(-(\beta + g)/\tau)}. \end{aligned} \quad (8)$$

Further, we denote $\beta = \log(\delta)$, and $\delta = \frac{\gamma}{1-\gamma}$. Thus, $\beta \in (-\infty, \infty)$, $\delta \in (0, \infty)$, $\gamma \in (0, 1)$, we have:

$$\gamma = \sigma(\beta), \quad (9)$$

and:

$$\hat{s}_t(\beta) = \frac{1}{1 + \exp(-((\log(\delta) + g)/\tau))}. \quad (10)$$

Following the definition in (Maddison et al., 2017), $\hat{s}(\beta) \in (0, 1)$ follows a Binary Concrete distribution, i.e., $\hat{s}(\beta) \sim \text{BinConcrete}(\delta, \tau)$ with location δ and temperature τ . As demonstrated in (Maddison et al., 2017), we have:

$$\begin{aligned} \mathbb{P}\left(\lim_{\tau \rightarrow 0} \hat{s}_t(\beta) = 1\right) &= \delta / (1 + \delta) \\ &= \frac{\gamma / (1 - \gamma)}{1 + \gamma / (1 - \gamma)} = \gamma \\ &= \sigma(\beta), \end{aligned} \quad (11)$$

which is the Bernoulli distribution variables in Eq. (6) of the main body of this paper.

A.6. Notations summary

We provide a comprehensive summary of the notations used throughout this paper in Table 2, facilitating a clear understanding of the mathematical formulations and concepts presented.

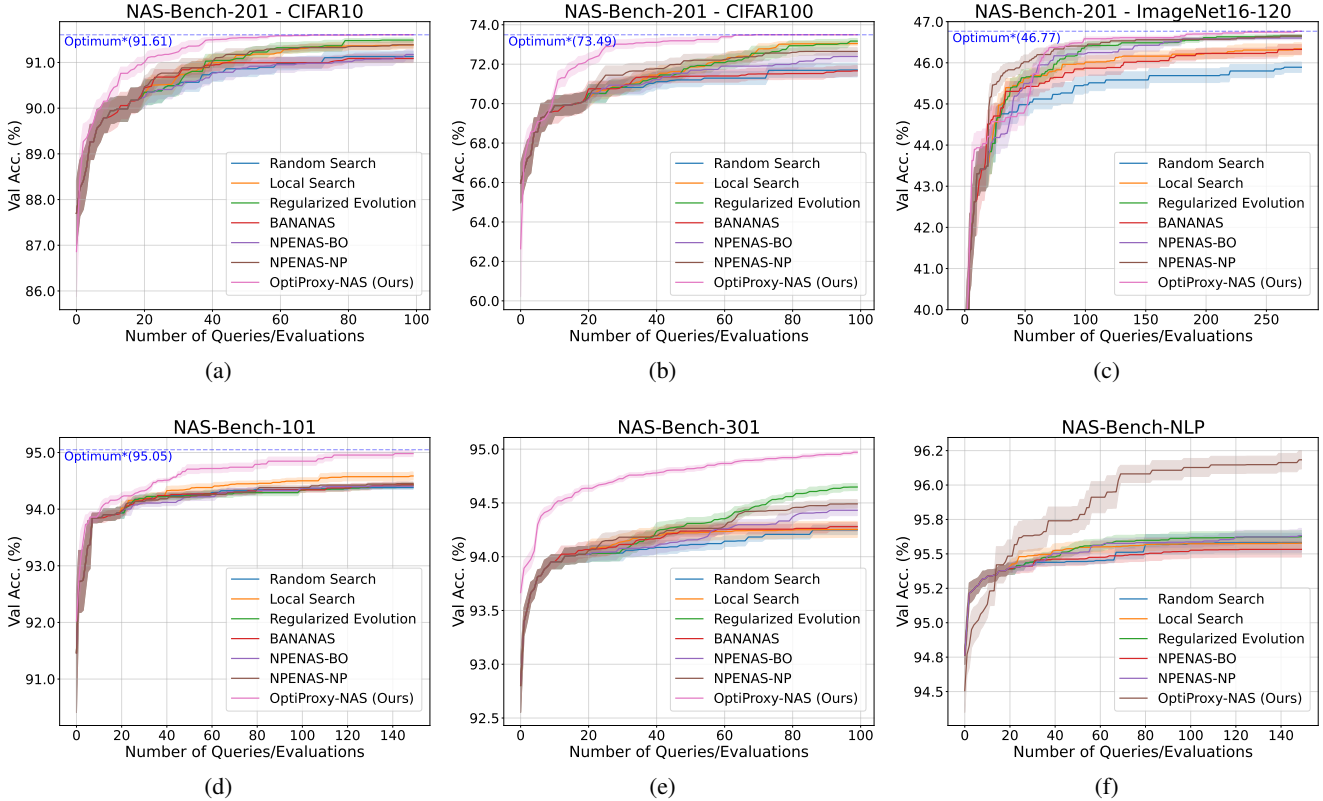


Figure 3: The trajectories in each subplot illustrate the statistics of the best-so-far values versus the query number across 10 random seeds. The solid lines represent the mean values, and the shaded areas indicate the standard error.

A.7. Experiments

A.7.1. EXPERIMENT SETUP

Our detailed experimental setup is as follows:

- **Benchmarks:** Following the standard practice in NAS algorithm comparisons, we choose the well-known benchmark datasets, including NAS-Bench-101, NAS-Bench-201, NAS-Bench-301, NAS-Bench-NLP, and HW-NAS-Bench, which spans 7 tasks of 4 search spaces across 3 different domains including computer vision, natural language processing, and resource-constrained NAS. For the types and structure of proxy models (neural networks), we employ the XGBoost as the surrogate model, also consistent with other comparison methods, e.g., AG-Net and DiNAS. Related versions are also maintained consistently: ▶ NAS-Bench-201: V1.0, ▶ NAS-Bench-301: V0.9; ▶ HW-NAS-BENCH: V1.0. In addition, surrogate model choice of surrogate benchmarks: ▶ NAS-Bench-301: XGBoost; ▶ NAS-Bench-NLP: svd_lgb.
- **Comparison methods:** We choose the SOTA methods in terms of sample efficiency under the mainstream

search strategies, details in Table 3.

- **Comparison metrics:** Following convention, we focus on the accuracy of the best architecture obtained (e.g., search based on validation accuracy) and queries cost, which directly determine the expenses of the entire search pipeline. We conduct experiments with 10 different seeds (0 ~ 9) and report the mean and standard deviation values (comparison methods typically report only the mean value).
- **Dataset setting:** The settings for the benchmark dataset include the version number, the search metric (val), whether to use the mean of the multi-seed training results or a single-seed result as the metric, and other settings. We ensure alignment with the latest SOTA comparison methods, AG-Net and DiNAS.
- **Reproducibility:** Following the comparative methodology, all experiments run with the random seeds from 0 to 9. We present the detailed reproducibility settings in the Appendix Section A.9.

Table 2: Notation Table

Symbol	Description
\mathbb{S}	The discrete NAS search space
\mathcal{X}	The continuously relaxed NAS search space spanning by α and β , proxy space
\mathcal{A}	Architecture in \mathbb{S}
α	The continuous operation feature variable of architecture (the unnormalized-logit value of the probability of the candidate operation)
β	The continuous topological structure of architecture (the Log-odds value of the connection probability between operation nodes)
γ	Connection probability between operation feature nodes
δ	The odds, how likely the connection exists
g	The i.i.d samples drawn from Gumbel distribution
τ	Temperature parameter in Gumbel softmax distribution
f	Landscape function
\hat{f}	Proxy model function
θ	Weights or parameters of the proxy model
θ^*	Optimal weights or parameters of the proxy model
\mathcal{A}^*	Optimal architecture
$\mathcal{A}_o, \mathcal{A}_t$	The topological structure and features variables (candidate operation choices)
\mathcal{L}	Loss function
\mathcal{D}	Sampled dataset $\{(\mathcal{A}_i, f(\mathcal{A}_i))\}_{i=1}^n$
s	Sampling process from the continuous probability distribution to discrete architecture
\hat{s}	Proxy sampling function
\hat{s}_o, \hat{s}_t	Soft embeddings of the topological structure and features variables
i, j	Feature nodes index and candidate operation index
h, k	Current and another feature nodes index
$\psi(\cdot)$	Objective function
$\sigma(\cdot)$	Sigmoid function
$\text{Cat}(\cdot)$	Categorical distribution
$\text{Bernoulli}(\cdot)$	Bernoulli distribution
N	The No. of feature nodes
M	The candidate operation number
C	The maximum query time cost
Q	The sampled candidate architectures number of each search step
B	The evaluation (quer) architecture number of each search step
λ	The ranking loss weight coefficient

A.7.2. QUERY EFFICIENCY EXPERIMENT

We present the query efficiency experiment in Figure 3. We choose the baseline methods that are incorporated in repo: <https://github.com/automl/NASLib>, under the compat-

Table 3: Comparison of NAS Algorithm Categories

Category	Comparison Methods
Random Search (RS)	(Li & Talwalkar, 2019)
Evolutionary Algorithms (EA)	Regularized Evolution (Li & Talwalkar, 2019)
Reinforcement Learning (RL)	Arch2vec+RL (Yan et al., 2020)
Local Search (LS)	(White et al., 2021b)
Predictor-based NAS	WeakNAS (Wu et al., 2021)
Supernet-based NAS	SGNAS (Huang & Chu, 2021), β -DARTS (Ye et al., 2022)
Generative NAS	NAO (Luo et al., 2018), GA-NAS (Rezaei et al., 2021), DiffusionNAG (An et al., 2023), DiNAS (Asthana et al., 2024), AG-Net (Lukasik et al., 2022)
Bayesian Optimization (BO)	BANANAS [†] (White et al., 2021a), Bayesian Opt. (Snoek et al., 2015), Arch2vec+BO (Yan et al., 2020)

ible search space, encoding scheme, and prediction models. Specifically, for tabular benchmarks (NAS-Bench-101 and NAS-Bench-201), our method demonstrates superior query efficiency. For the surrogate benchmarks (NAS-Bench-301 and NAS-Bench-NLP), we consistently outperform the baseline methods along with the increase in query numbers. Specifically, we ignore the running of BANANAS on NAS-Bench-NLP due to its incompatible path encoding scheme.

A.7.3. VISUALIZATION

We visualize the search space of NAS-Bench-201, CIFAR-10 to demonstrate the properties of the search space and the effectiveness of the proposed method using the search trajectory, as Figure 4. We perform PCA on these embeddings to reduce the dimensionality from 5 to 2 and add the validation accuracy as the third dimension to further differentiate the architectures based on their performance, as shown in Figure 4a. Typically, our method demonstrated significant efficiency during the first few evaluations, the search could be led to the advantageous region quickly. So we zoom in on this region (the region of red points) for a closer look. To better differentiate the performance of the architectures in this region we use a more focused color-bar in this graph and view the space in $-y$ direction and the three-dimensional space landscape visualization, as Figure 4b and Figure 4c, respectively.

A.8. Search Spaces Parameterization and Encoding schemes

A.8.1. NAS-BENCH-201.

We present the illustration of the NAS-Bench-201 space and encoding scheme in Figure 5. The architecture in NAS-Bench-201 space has a fixed topological structure, as shown in Figure 5a. The NAS targets the operation choice from the candidate operations set, with the entire space comprising $6^5=15,625$ architectures. The embedding scheme of NAS-Bench-201 can be summarized: ► The α is as Fig-

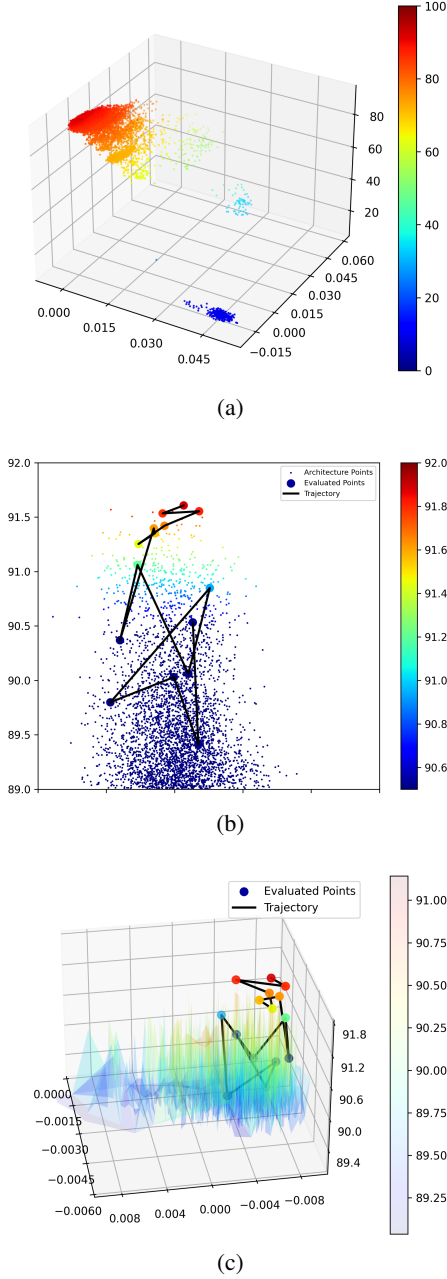


Figure 4: Visualization of the search space architecture distribution and search trajectory on NAS-Bench-201 (CIFAR-10). (a) Overview of the search space using PCA. (b) The primary exploration region of our method, viewed from the y -direction, with a specific area zoomed in for detail. For clarity, only the best architecture point out of every five evaluated architectures is visualized. This illustration search takes 70 queries to reach the global optimum. Based on our observations, every 10 evaluations yield a new best architecture. (c) The search trajectory within the spiky search space landscape.

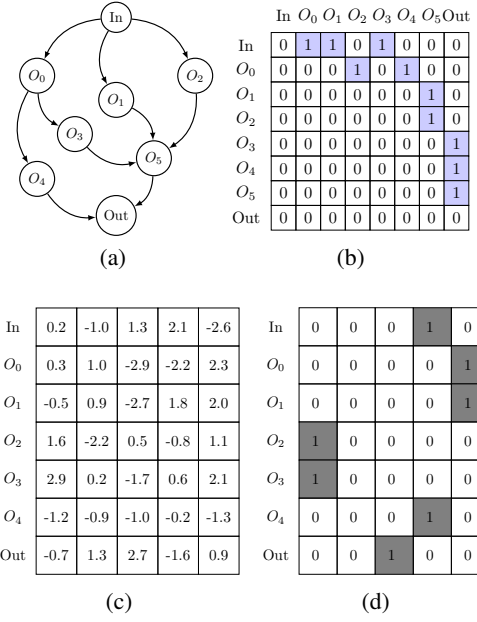


Figure 5: (a) Illustration of search space of NAS-Bench-201. (b) The fixed topological structure (adjacency matrix) of the architecture cell. (c) The relaxed architecture operation feature variables α . (d) The hard embedding of the topological structure that is sampled architecture based on α .

Figure 5c, within the range of \mathbb{R} . For hard embedding after the sampling s , adjacency matrix and operation feature are as Figure 5b and Figure 5d, respectively. The candidate operation set in NAS-Bench-201 space is as follows:

```
opname_to_index = {
    'none': 0,
    'skip_connect': 1,
    'conv_1x1': 2,
    'conv_3x3': 3,
    'avg_pool_3x3': 4
}
```

We further analyze the impact of operations on the topological structure. Given the original Figure 6a, we further discuss the vibrations over the operation selection change: When “skip_connect” is chosen, it changes the topological structure, represented as an adjacency matrix, as illustrated in Figure 6b. When “none” is chosen, the adjacency matrix is also affected, as illustrated in Figure 6c. We consider that these coupling factors between the operation matrix and the adjacency matrix can be neglected, that is, the adjacency matrix of this architectural space always exists in a fixed form as Figure 5b, which is also the commonly employed encoding method for this space in the NAS community.

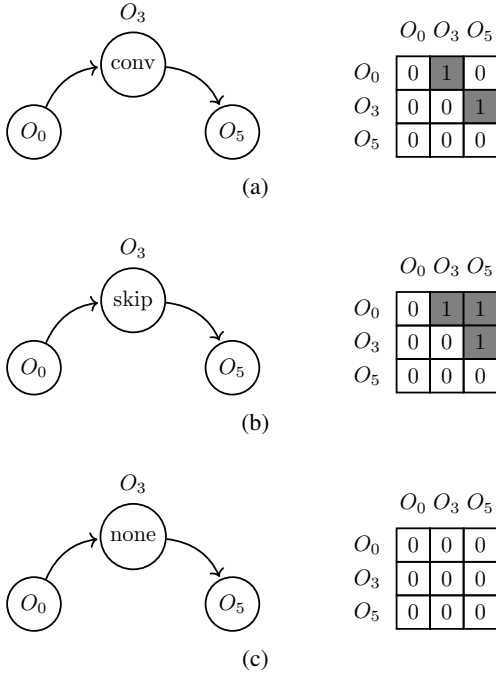


Figure 6: From the perspective of graph structure, illustration of the coupling relationship between operation choice and adjacency matrix. (a) The original connectivity pattern when the operation choice is “conv_3x3”. (b) When the “skip_connect” is chosen, the edge originating from O_3 and connecting to O_3 will both be removed, and a new edge is additionally added to bypass the node O_3 , resulting in the change of the adjacency matrix. (c) When the “none” is chosen, the edge originating from O_3 and connecting to O_3 will both be removed, resulting in the zero out of the adjacency matrix element.

A.8.2. NAS-BENCH-101.

We present the illustration of the NAS-Bench-101 space and encoding scheme in Figure 7, both topological structure and operation features are to be searched. The embedding scheme of NAS-Bench-101 can be summarized: ▶ The α is as the type of Figure 5c of NAS-Bench-201, and the form of β is as Figure 7b, each element is within the range of \mathbb{R} . ▶ For hard embedding after the sampling s , the adjacency matrix is as Figure 7c. The candidate operation set of NAS-Bench-101 space is as follows:

```
opname_to_index = {
    'conv3x3-bn-relu': 0,
    'conv1x1-bn-relu': 1,
    'maxpool3x3': 2
}
```

Critically, the NAS-Bench-101 space imposes the following validity constraints on the architecture: ▶ The edge number

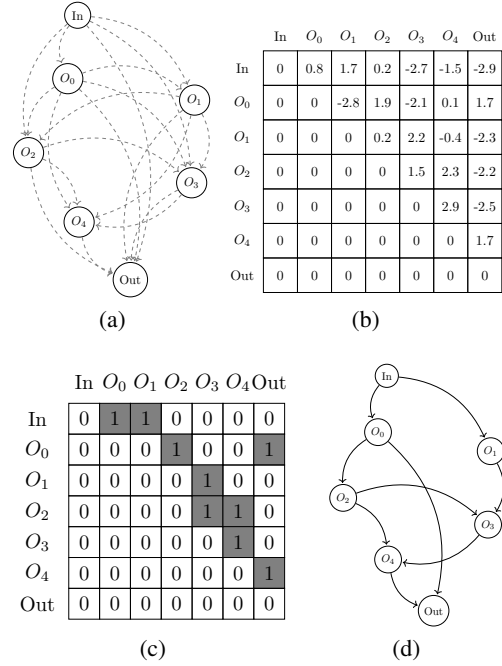


Figure 7: Illustration of the search space of NAS-Bench-101. (a) The architecture cell of NAS-Bench-101. Both topological structure (edges represented by dashed line) and operation features (nodes) are to be searched. (b) β in continuous space. (c) The encoding scheme (hard embedding) of graph topology structure that is sampled based on β . (d) The graph of sampled candidate architecture.

▶ At least one emanates from an In node. ▶ At least one node outputs to the Out node. Additionally, due to the collaborative changes and coupling relationship of the topological structure and node features in network architecture, isomorphic graphs exist in the space (Ying et al., 2019): ▶ The two architectures have different adjacency matrices or node features, but are computationally equivalent. ▶ The vertices not on a path from the input vertex to the output vertex do not contribute to the computation, so such vertices being pruned will not result in a different architecture cell. Considering the isomorphic graphs, NAS-Bench-101 consists of $\sim 423K$ unique architectures. For simplicity, the hard embeddings and soft embeddings of operation features are the same as NAS-Bench-201, we ignore the detailed description here. To be noticed, the nature of ‘validity constraints’ and ‘isomorphic graphs’ brings up challenges to our independent and unconstrained optimization of topological structure and operation features. We address this issue by deduplication, validity verification, and repeated sampling attempts. Interested readers are advised to refer to our implementation code.

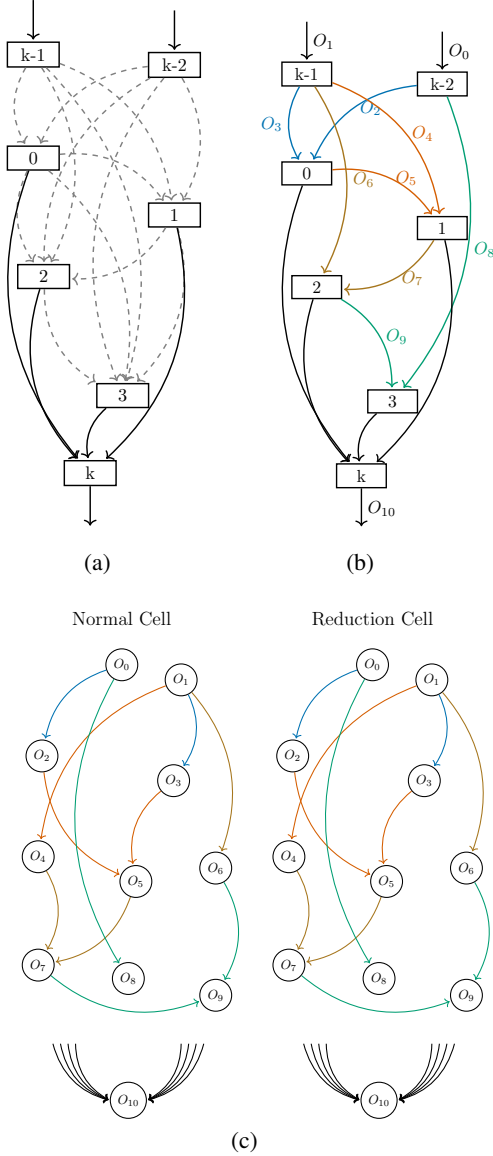


Figure 8: Illustration of the search space of NAS-Bench-301. (a) The original schematic of the searched architecture cell, in the view of feature maps as the nodes and operations as the edge. The topological structure (edges represented by dashed line) and operation features (nodes) are to be searched, both for “Normal cell” and “Reduction cell”; (b) The sampled architecture cell with 2 preceding feature maps (nodes); (c) The transformed graph representation with nodes representing operations and edges standing for the feature maps.

A.8.3. NAS-BENCH-301.

The candidate operation set of NAS-Bench-101 space is as follows:

	O_0	O_1	O_2	O_3	O_4	O_5	O_6	O_7	O_8	O_9	O_{10}
O_0	0	0	1	0	0	0	0	0	1	0	0
O_1	0	0	0	1	1	0	1	0	0	0	0
O_2	0	0	0	0	0	1	0	0	0	0	1
O_3	0	0	0	0	0	1	0	0	0	0	1
O_4	0	0	0	0	0	0	0	1	0	0	1
O_5	0	0	0	0	0	0	0	1	0	0	1
O_6	0	0	0	0	0	0	0	0	0	1	1
O_7	0	0	0	0	0	0	0	0	0	1	1
O_8	0	0	0	0	0	0	0	0	0	0	1
O_9	0	0	0	0	0	0	0	0	0	0	1
O_{10}	0	0	0	0	0	0	0	0	0	0	0

Figure 9: The illustration of the adjacency matrix of the sampled architecture. The elements with the blue background represent fixed edges, while elements with the lightgray background represent edge choices through sampling.

Table 4: Candidate Preceding Nodes (Groups)

Node	Candidate Preceding Nodes (Groups)	Selection num
O_2	$\{O_0\}$	1
O_3	$\{O_1\}$	1
O_4	$\{\{O_0\}, \{O_1\}\}$	1
O_5	$\{\{O_1\}, \{O_2, O_3\}\}$	1
O_6	$\{\{O_0\}, \{O_1\}, \{O_2, O_3\}\}$	1
O_7	$\{\{O_1\}, \{O_2, O_3\}, \{O_4, O_5\}\}$	1
O_8	$\{\{O_0\}, \{O_1\}, \{O_2, O_3\}, \{O_4, O_5\}\}$	1
O_9	$\{\{O_1\}, \{O_2, O_3\}, \{O_4, O_5\}, \{O_6, O_7\}\}$	1

```
opname_to_index = {
    'skip_connect': 0,
    'max_pool_3x3': 1,
    'avg_pool_3x3': 2,
    'sep_conv_3x3': 3,
    'sep_conv_5x5': 4,
    'dil_conv_3x3': 5,
    'dil_conv_5x5': 6
}
```

The space of NAS-Bench-301 is vast, containing $\sim 10^{18}$ architectures, many orders of magnitude larger than any previous tabular NAS benchmark. For the scale of search space, surrogate models (XGBoost, GIN and LGBost) are employed to make it as surrogate benchmarks. To note, for the types and structure of proxy models (neural networks), we employ the XGBoost as the surrogate model for experiments, keeping compliant with comparison methods. We present the search space illustration in Figure 9. The original schematic of the searched architecture cell is presented as the directed acyclic graph (DAG), in the view of feature maps as the nodes and operations as the edge. The design of NAS-Bench-301 allows a node to select two of its preceding nodes as its input nodes, as in Figure 8b. To keep

	O_0	O_1	O_2	O_3	O_4	O_5	O_6	O_7	O_8	O_9	O_{10}
O_0	0	0	1	0	0.3	0	2.3	0	0.3	0	0
O_1	0	0	0	1	0.2	0.7	1.2	2.1	0.5	-0.5	0
O_2	0	0	0	0	0	0.5	0.4	0.5	0.9	0.6	1
O_3	0	0	0	0	0	-0.1	0.9	0.2	0.1	0.4	1
O_4	0	0	0	0	0	0	0	0.6	0.03	0.9	1
O_5	0	0	0	0	0	0	0	0.05	0.4	1.3	1
O_6	0	0	0	0	0	0	0	0	1.3	1.7	1
O_7	0	0	0	0	0	0	0	0	0	0.2	1
O_8	0	0	0	0	0	0	0	0	0	0	1
O_9	0	0	0	0	0	0	0	0	0	0	1
O_{10}	0	0	0	0	0	0	0	0	0	0	0

(a) The relaxed topological structure variables β ;

	O_0	O_1	O_2	O_3	O_4	O_5	O_6	O_7	O_8	O_9	O_{10}
O_0	0	0	1	0	0.93	0	0.81	0	0.38	0	0
O_1	0	0	0	1	0.98	0.75	0.67	0.43	0.86	0.40	0
O_2	0	0	0	0	0	0.98	0.32	0.95	0.72	0.74	1
O_3	0	0	0	0	0	0.52	0.82	0.67	0.64	0.83	1
O_4	0	0	0	0	0	0	0	0.80	0.69	0.87	1
O_5	0	0	0	0	0	0	0	1.00	0.97	0.89	1
O_6	0	0	0	0	0	0	0	0	0.74	0.78	1
O_7	0	0	0	0	0	0	0	0	0	0.21	1
O_8	0	0	0	0	0	0	0	0	0	0	1
O_9	0	0	0	0	0	0	0	0	0	0	1
O_{10}	0	0	0	0	0	0	0	0	0	0	0

(b) The soft embedding of \hat{s}_t based on the propagation from β , based on a simulative calculation with a temperature of 0.7;

Figure 10: The proxy sampling of topological structure variables in NAS-Bench-301. The colored boxes represent edge groups transformed based on the proceeding nodes relationship.

the compatible encoding scheme and facilitate the search, we transform the representation of the graph so that nodes represent operations and edges stand for the feature maps, as in Figure 8c. First, the precedence relationships of the feature maps need to be converted into the precedence relationships of the operation nodes, as in Table 4, commonly, one of the proceeding nodes group is to be selected as the input node. Thus, given this transformation, we need to reconstruct the implementation logic of the original discrete sampling function w.r.t the topological structure, as well as the forward propagation logic of the proxy sampling propagation. Given the relaxed topological structure variables β in Figure 10a, which is constructed based on Table 4: ► For proxy sampling propagation, the soft embedding of \hat{s}_t propagation based on β , as Figure 10b. ► For the discrete

	O_0	O_1	O_2	O_3	O_4	O_5	O_6	O_7	O_8	O_9	O_{10}
O_0	0	0	1	0	0.57	0	0.91	0	0.57	0	0
O_1	0	0	0	1	0.55	0.67	0.77	0.89	0.66	0.38	0
O_2	0	0	0	0	0	0.55	0.65	0.59	0.66	0.63	1
O_3	0	0	0	0	0	0.55	0.65	0.59	0.52	0.63	1
O_4	0	0	0	0	0	0	0	0.58	0.52	0.75	1
O_5	0	0	0	0	0	0	0	0.58	0.70	0.75	1
O_6	0	0	0	0	0	0	0	0	0.70	0.70	1
O_7	0	0	0	0	0	0	0	0	0	0.70	1
O_8	0	0	0	0	0	0	0	0	0	0	1
O_9	0	0	0	0	0	0	0	0	0	0	1
O_{10}	0	0	0	0	0	0	0	0	0	0	0

(a) The adjacency matrix with the mean value of group-wise elements after $\sigma(\beta)$ propagation;

	O_0	O_1	O_2	O_3	O_4	O_5	O_6	O_7	O_8	O_9	O_{10}
O_0	0	0	1	0	1	0	1	0	0	0	0
O_1	0	0	0	1	0	1	0	1	0	0	0
O_2	0	0	0	0	0	0	0	0	0	0	1
O_3	0	0	0	0	0	0	0	0	0	0	1
O_4	0	0	0	0	0	0	0	0	0	1	1
O_5	0	0	0	0	0	0	0	0	1	1	1
O_6	0	0	0	0	0	0	0	0	1	0	1
O_7	0	0	0	0	0	0	0	0	0	0	1
O_8	0	0	0	0	0	0	0	0	0	0	1
O_9	0	0	0	0	0	0	0	0	0	0	1
O_{10}	0	0	0	0	0	0	0	0	0	0	0

(b) The hard embedding with sampling s_t function following the $\sigma(\beta)$;

Figure 11: The discrete sampling of topological structure variables in NAS-Bench-301.

sampling function, the sigmoid propagation is element-wise, followed by the mean operation of group-wise elements, as Figure 11a. Then the discrete sampling is based on the mean value of the groups, as Figure 11b. ► In terms of the chain-style structure with “Normal cell” and “Reduction cell” in NAS-Bench-301, we merge the two adjacency matrices as Figure 12, combined with the concatenation of two operation feature matrices, as a fusion graph for propagation.

Based on our practice, this transform strategy and encoding scheme of NAS-Bench-301 is meticulously designed but also reliable, reasonable, and effective. We recommend that readers refer to our code implementation. In addition, for simplicity, the hard embedding and soft embedding of operation features are the same as NAS-Bench-201 and NAS-Bench-101, we ignore the detailed description here.

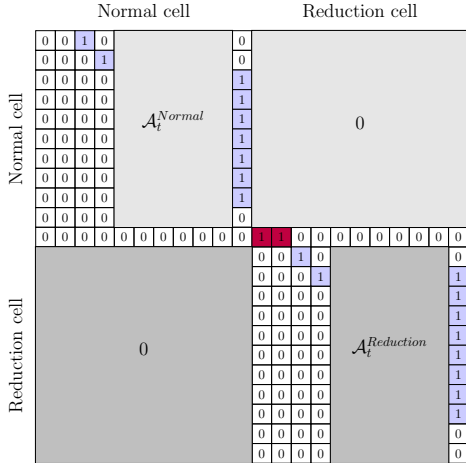


Figure 12: The combination of adjacency matrices of “Normal cell” and “Reduction cell”, as an integrated graph structure.

A.8.4. NAS-BENCH-NLP.

NAS-Bench-NLP benchmark results from the recurrent neural network space. We keep the graph structure encoding scheme for NLP in the NASLib library unchanged, and do not specially design the discrete sampling function and proxy sampling propagation. Given the detailed descriptions of the aforementioned search spaces, we do not elaborate further here and recommend interested readers to examine the code.

A.9. H. Hyperparameter and Reproducibility

In this section, we provide the hyperparameter settings and tuning experiences in our experiments. Overall, they are divided into two parts: Model Fitting and Search and sampling. For the same search space, the fitting parameters of the surrogate model generally remain consistent. However, for different search spaces, it is necessary to adjust the scale of the surrogate model based on the complexity of the space’s graph structure, as well as the encoding schemes. Importantly, search and sampling parameters need to be empirically adjusted according to the space scale, query cost budget, and other factors. When dealing with real NAS tasks, hyperparameters can be adjusted using surrogate tasks or proxy metrics, e.g., early stop training criteria, or small-scale proxy task datasets. For instance, when transferring the hyperparameters setting for CIFAR-10 to CIFAR-100 and ImageNet16-120, the search results are still satisfactory.

A.9.1. HYPERPARAMETER SETUP AND TUNING EXPERIENCE

We present the hyperparameters example of model fitting in Table 5. Accordingly, we provide the following hyperparam-

Table 5: Model fitting hyperparameters

Parameter	Value	Description
<i>gcn_hidden</i>	144	No. of neurons in a GCN layer
<i>gcn_layers</i>	2	No. of GCN layers
<i>linear_size</i>	144	No. of neurons in the MLP
<i>batch_size</i>	7	Batch size
<i>optimizer</i>	AdamW	Optimizer for training
<i>lr</i>	0.001	Learning rate
<i>model_epochs</i>	100	No. of training epochs
<i>ranking_coe</i>	0.2	Coefficient for ranking loss
<i>m</i>	0.1	Ranking loss margin
<i>lr_scheduler</i>	exponential	Learning rate scheduler
<i>lr_gamma</i>	0.9	Decay rate of the lr scheduler
<i>lr_step</i>	10	Step size of learning rate decay

Table 6: Search and sampling hyperparameters

Parameter	Value	Description
<i>base_temp</i>	0.7	Highest temperature
<i>min_temp</i>	0.2	Lowest temperature
<i>lr_alpha</i>	0.02	Learning rate for α
<i>lr_beta</i>	0.001	Learning rate for β
<i>search_epochs</i>	300	Optimizing epochs of each step
<i>o_epochs</i>	15	Optimization interval epochs for α
<i>t_epochs</i>	15	Optimization interval epochs for β
<i>optimizer1</i>	AdamW	Optimizer for α
<i>optimizer2</i>	AdamW	Optimizer for β
<i>parallel_batch</i>	5	(α, β) groups No. (K)
<i>num_sample</i>	10	Samples No. of each step
<i>num_sample_init</i>	10	Initially random samples No.
<i>search_steps</i>	9	No. of search steps
<i>lhs_lower</i>	0.9	The lower bound for LHS
<i>lhs_range</i>	0.1	The range bound for LHS
<i>verify_ratio</i>	20	Selection ratio (Q/K)

eter tuning insights: ▶ The number of GCN layers affects the range of message passing, a significant increase in the GCN layers will cause over-smoothing. Under our framework, across all the NAS tasks, two layers are sufficient. ▶ Typically, a reasonably bigger *batch_size* is better. If you aim to evaluate 100 architectures in total, set *batch_size* to 20 is adequate. But a large *batch_size* complicates ranking loss calculations, increasing the time consumption; ▶ As for *model_epochs*, according to our practice, for common search spaces, 100 training epochs are sufficient for prediction performance. ▶ Setting the *ranking_coe* too high may bias the model predictions, while setting it too low may fail to preserve the prediction ranking performance. We present the hyperparameters example of architecture search (gradient-based optimization) and sampling in Table 6. Accordingly, we provide the following hyperparameter tuning insights: ▶ The temperature in Gumbel-Softmax can influence the randomness of the sampling. The predefined highest *base_temp* affects the exploration in the early stages of the search, within a range of $[0, \infty]$. Based on our

experience, it is commonly set to $[0.5, 1]$, which is considered appropriate. The *min_temp* determines the unbiased nature of the proxy gradient and the original gradients, commonly set close to 0. ▶ The learning rate for α and β , their decay rate, and the Gumbel temperature must be empirically co-adjusted. If a particular operation or topological edge selection dominates from the outset, exploration should be encouraged, for example, by lowering the learning rate and increasing the range of temperature values. ▶ The *parallel_batch* controls the group number of (α, β) . Increasing it encourages exploration, but setting it significantly higher than *num_sample* is forbidden. *num_sample_init* controls the number of points randomly sampled in the first search step. A large *num_sample_init* can avoid local minima but may reduce efficiency. ▶ The *verify_ratio* determines the number of samples following (α, β) , that is the selection ratio Q/K . ▶ During the initialization of the alphas, we use LHS to initialize them, with *lhs_range* controlling their separation.

A.9.2. ENVIRONMENT DETAILS AND REPRODUCIBILITY

Our hardware and software specs are:

```
CPU: 13th Gen Intel Core i7-13700K
RAM: 128GB DDR5@5200MT/s
GPU: NVIDIA RTX 4090@2775MHz
Kernel: Linux 6.2.0-31-generic
NVIDIA Driver Version: 535.104.05
NVML Version: 12.535.104.05
CUDA Version: 11.8
PyTorch Version: 2.0.0
```

Our experimental code is based on the repo of <https://github.com/automl/NASLib>, which involves the search space, dataset settings, original discrete encoding schemes, and data preprocessing from this excellent open-source library. This also facilitates our subsequent open-source contributions and future community engagement. The code will be released at <https://github.com/blyucs/OptiProxy-NAS>. Python environment details are provided in a requirement file. If you have difficulty reproducing our work, please don't hesitate to contact us.